Available online at www.sciencedirect.com

ScienceDirect

journal homepage: www.elsevier.com/locate/he

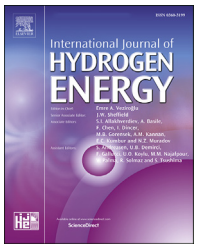

Optimization of power allocation for wind-hydrogen system multi-stack PEM water electrolyzer considering degradation conditions

Xinyu Lu [a], *Banghua Du* [b], *Shenpei Zhou* [a], *Wenchao Zhu* [b], *Yang Li* [a], *Yang Yang* [a], *Changjun Xie* [a,b,*], *Bo Zhao* [c,**], *Leiqi Zhang* [c], *Jie Song* [d], *Zhanfeng Deng* [d]

[a] *School of Automation, Wuhan University of Technology, Wuhan 430070, China*
[b] *School of Automotive Engineering, Wuhan University of Technology, Wuhan 430070, China*
[c] *State Grid Zhejiang Electric Power Research Institute, Hangzhou 310014, China*
[d] *Global Energy Interconnection Research Institute, Beijing 102211, China*

HIGHLIGHTS

- Multi-physics fields three-dimensional model of the PEM water electrolyzer (PEMWE).
- Quantification of PEMWE degradation by voltage degradation rate.
- The wind-hydrogen system energy efficiency is 61.65%, and the PEMWE single-stack voltage degradation is 7.5 V.
- Power allocation execution module current ripple is 0.053% of output current with excellent signal following capability.

ARTICLE INFO

Article history:
Received 9 September 2022
Received in revised form
14 October 2022
Accepted 9 November 2022
Available online 7 December 2022

Keywords:
Wind-hydrogen system
Power allocation
PEM water electrolyzer
Voltage degradation rate
Energy efficiency
Extended duty cycle interleaved buck converter

ABSTRACT

Hydrogen production from wind power has become one of the most important technologies for the large-scale comprehensive development and utilization of wind power, but the randomness of wind power has a large negative impact on the stability and cost of such wind-hydrogen hybrid energy systems. In this work, we initially analyze the relationship between electrolyzer efficiency and degradation with a three-dimensional multi-physics field model of PEMWE single-cell. Optimization of a power allocation strategy for wind-hydrogen system with a multi-stack PEM water electrolyzer (PEMWE) is proposed by considering degradation conditions. The multi-stack PEMWE power allocation strategy consists of the control module and execution module. In the control module, the degradation of PEMWE is quantified using the voltage degradation rate under different operating conditions. By setting the turning power point and external power supply and calculating the power allocation order online to reduce the degradation of PEMWE. In the execution module, the extended duty cycle interleaved buck converter (EDCIBC) based on fuzzy PID control is used to power each PEMWE single-stack. Case studies are carried out via computer simulation based on the configuration and experimental data for a specific wind farm located in Cixi, Zhejiang, China. Our results show that the energy efficiency of the wind-hydrogen system is 61.65% in a one-year operation, the voltage degradation of the

* *Corresponding author.*
** *Corresponding author.*
E-mail addresses: jackxie@whut.edu.cn (C. Xie), zhaobozju@163.com (B. Zhao).
https://doi.org/10.1016/j.ijhydene.2022.11.092

PEMWE single-stack is 7.5 V, and the maximum efficiency is 6.29% lower than that when it is not aged. The EDCIBC output current ripple is as low as 0.053%, which rapidly and accurately follows the generated power allocation signal.

Nomenclature

Abbreviations

PEMWE	Proton Exchange Membrane Water Electrolyzer
EDCIBC	Extended Duty Cycle Interleaved Buck Converter
AE	Alkaline Electrolyzer
AEMWE	Anion Exchange Membrane Water Electrolyzer
SOE	Solid Oxide Electrolyzer
AST	Accelerated Stress Test
PEM	Proton Exchange Membrane
BP	Bipolar Plate
GDL	Gas Diffusion Layer
CL	Catalytic Layer

Symbols

V_{cell}	PEMWE single-cell voltage, V
V_{oc}/V_{th}	open-circuit/thermoneutral voltage, V
$V_{act}/V_{con}/V_{ohm}$	activation/concentration/ohmic overpotential, V
R	universal gas constant, J/(mol·K)
F	Faraday constant, C/mol
T	operating temperature, K
p	operating pressure, Pa
a	material activity
E_0	standard electric potential, V
i	current density, A/cm^2
i_0	exchange current density, A/cm^2
c	concentration, mol/cm^3
A	activated membrane area, cm^2
R	ohmic resistance, Ω
R_{in}	resistance of the ion passing through the membrane, Ω
v	volume average velocity, cm^3/s
s	mass source term
d	diffusion coefficient
C	heat capacity, J/K
P	power, W
V	voltage, V
I	current, A
n	cell number
k	operating electrolyzers number
P_{wind}	wind power, W
P_k	start-stop power point, W
P_t	turning power point, W
$V_m/V_{fl}/V_{ct}/V_{fh}/V_{cr}$	voltage degradation rate under different operating conditions, V
$t_m/t_{fl}/t_{ct}/t_{fh}/t_{cr}$	operating times under the corresponding operating conditions, h
K	electrolyzers total number
N	production rate m^3/h
Δi_o	current ripple, A
R	voltage ratio
V_S	switching device voltage stress, V
L	inductor, mH
D	switching device duty cycle
f_s	switching device switching frequency, Hz
V_{dc}/V_o	input/output voltage of MIBC, V
$K_p/K_i/K_d$	PID controller parameters
E	difference
EC	change rate of E
P_{ref}	system allocation power signal

Greek Symbols

α	charge transfer coefficient
δ	thickness, μm
σ	ion conductivity, S/m
λ	water content
ε	porosity
μ	viscosity, Pa s
ρ	average density, g/cm^3
η	efficiency, %
γ	thermal conductivity, W/(m·K)

activated membrane area cm^2

Subscripts

0	reference value
O_2	oxygen
H_2	hydrogen
H_2O	water
an	anode
cat	cathode
mem	membrane
f	fluid mixture
s	solid area
m	m-th material phase
eff	effective value
ae	auxiliary equipment
el	electrolyzer

Introduction

Wind power is one of the most mature and commercialized renewable energy generation technologies [1]. According to the Global Wind Energy Council, the cumulative global installed capacity of wind power reached 837 GW in 2021, with a yearly increase rate of 12.3% [2]. However, wind power is intermittent and random, and in some time of periods, it needs to be curtailed to prevent a negative impact on the power grid, resulting in a significant underutilization of wind energy [3]. Hydrogen, with a high energy density and convenience for storage and transportation, has become an important media for the large-scale, comprehensive development of next-generation wind power systems [4]. In addition, a plethora of investigations from different countries and regions have also proved the technical and economic feasibility of large-scale wind power hydrogen production [5–10].

Conventional hydrogen production by water electrolysis operates at a fixed hydrogen production rate under a stable power supply from conventional (e.g. fossil-fuelled) power generation, which is very costly. Combining wind power with water electrolysis for hydrogen production can improve the utilization rate of wind power and reduce the cost of hydrogen production at the same time [11]. There are four main types of water electrolyzers: alkaline electrolyzer (AE), proton exchange membrane water electrolyzer (PEMWE), anion exchange membrane water electrolyzer (AEMWE), and solid oxide electrolyzer (SOE). While the AE technology is mature and widely used, there are some disadvantages such as low current density, gas impurities, slow system response, and environmental pollution [12]. A PEMWE adopts a zero-pitch structure and conducts protons through the polymer membrane. Because the movement of protons on the polymer membrane responds rapidly to power fluctuations, the PEMWE has good compatibility with wind power and photovoltaic and is conducive to rapid load change [13–15]. Although AEMWE theoretically combines the benefits of AE and PEMWE, anion exchange membranes are difficult to prepare, have low hydroxide conductivity and poor chemical stability, and currently do not meet commercial requirements [16–18]. The SOE is also a promising technology, but due to severe degradation of the reactor at high temperatures and hydrogen safety issues, it has not yet been commercially viable and is still in the laboratory scale [19,20]. Combining the characteristics and development of various types of electrolyzers, PEMWE is increasingly being used in hydrogen-electric coupling demonstration projects, and has shown good results [21], so this work focuses on using PEMWEs to build the electrolyzer array for wind-hydrogen systems.

A number of studies have shown that frequent start-stop switching, power fluctuations, high-frequency current ripple, etc., will accelerate the degradations of PEMWE electrocatalysts and membrane, and aggravate metal ion poisoning [22,23]. A study by Chandesris et al. [24] investigated the effects of temperature and current density on membrane degradation by analyzing fluoride emissions during PEMWE runs. Frensch et al. [25] examined PEMWE performance and degradation under seven different operating conditions and concluded that dynamic operation led to catalyst support passivation accelerated. Weiss et al. [26,27] proposed a PEMWE Accelerated Stress Test (AST) method that simulates a fluctuating power supply, and they demonstrated the detrimental effects of frequent start-stop switching, power fluctuations, and long-term high-power operation on PEMWEs. Rakousky et al. [28] conducted experiments on five PEMWE single-cells and measured their degradation under both constant and intermittent power in order to determine how the PEMWE degradation rate changes under different working conditions. Guo et al. [29] summarized the power electronic converters under the scenario of hydrogen production using renewable energy and compared their static characteristics such as current ripple, voltage ratio, and voltage stress, concluded that the interleaved parallel converter topology has superior performance.

In the study of the power allocation for a multi-stack electrolyzer, we found that it is somewhat similar to the study of multi-stack fuel cells [30]. Muyeen et al. [31] developed a collaborative control system that pairs wind farms with 10 water electrolysis hydrogen production units in parallel, utilizing first-in-first-out (FIFO) algorithms to control the start-stop of each hydrogen production unit, thereby increasing system performance. Fang et al. [32] found that by installing supercapacitors in the wind-hydrogen system to absorb transient power and adopting a modular adaptive control strategy to optimize alkaline electrolyzer array operation, the number of electrolyzer start-stop switching could be significantly reduced and the system hydrogen production could be improved. Hong et al. [33] proposed an optimal scheduling method for wind-hydrogen systems considering efficiency optimization, using an artificial bee colony algorithm to solve for the optimal hydrogen production power and a segmented fuzzy control strategy to improve the overall efficiency of the alkaline electrolyzer array. Luxa et al. [34] established a multi-stack hydrogen production array consisting of 100 PEM electrolyzers and demonstrated its applicability under complex operating conditions by two control strategies.

In the above, we reviewed the existing and limited studies on the power allocation for wind-hydrogen system multi-stack electrolyzer array. Most of them focus on the alkaline electrolyzer, and ignores the impact of power fluctuations and frequent start-stop switching on the life of the electrolyzer. Furthermore, although some scholars have designed interleaved parallel converters with better performance as electrolyzer converters, the conventional Buck converter is still used as the execution module of the power allocation strategy in some system-level studies, with a large current ripple and small voltage conversion ratio, and poor performance in following the power allocation reference signal, which will lead to performance degradation in practical applications [29,35–39]. These research problems motivate us to investigate the optimization of power allocation for wind-hydrogen system multi-stack PEMWE considering degradation conditions in this work. We analyze the relationship between electrolyzer efficiency and degradation with a three-dimensional multi-physics field model of PEMWE single-cell. Optimization of a power allocation strategy for wind-hydrogen systems with a multi-stack PEMWE is proposed by considering degradation conditions. The multi-stack PEMWE

power allocation strategy consists of the control module and execution module. In the control module, the degradation of PEMWE is quantified using the voltage degradation rate under different operating conditions. By setting the turning power point and external power supply and calculating the power allocation order online to reduce the degradation of PEMWE. In the execution module, we apply fuzzy PID control to the extended duty cycle interleaved buck converter (EDCIBC) proposed by Pan et al. [37], being used to power each PEMWE single-stack. Case studies are carried out via computer simulation based on the configuration and experimental data for a specific wind farm located in Cixi, Zhejiang, China, verified the superiority of the designed solution.

To present our solution, the rest of this paper is organized as follows. Section Modeling and characterization of PEMWE analyzes the relationship between electrolyzer efficiency and degradation by building a multi-physics fields three-dimensional model of PEWME. Section Optimization of power allocation describes the structure and principles of power allocation for wind-hydrogen system multi-stack PEMWE considering degradation conditions. In Section Optimization of power allocation, the results obtained by the method proposed in this work are discussed. Conclusions are drawn in Section Conclusion.

Modeling and characterization of PEMWE

PEMWE uses a DC power supply as the input power source. As shown in Fig. 1, a single-cell of the PEMWE mainly consists of bipolar plates (BP), gas diffusion layers (GDL), catalytic layers (CL), and a proton exchange membrane (PEM). Liquid water enters the electrolyzer through the anode gas diffusion layer, oxygen produced by water electrolysis is precipitated from the anode, protons enter the cathode through the proton exchange membrane, electrons are transmitted by the external circuit, the protons through the PEM and the electrons transmitted by the external circuit combine to produce hydrogen [40]. The chemical reaction is governed by the following equations:

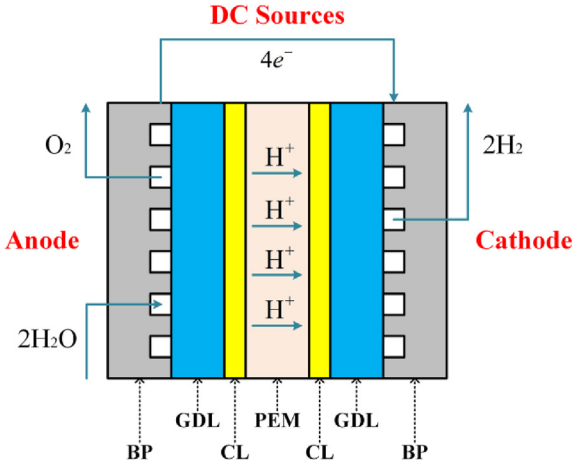

Fig. 1 – PEMWE single-cell structure and chemical reactions.

Anode reaction equation:

$$2H_2O(l) \rightarrow O_2(g) + 4H^+(aq) + 4e^- \quad (1)$$

Cathode reaction equation:

$$4H^+(aq) + 4e^- \rightarrow 2H_2(g) \quad (2)$$

PEMWE multi-physics fields three-dimensional modeling

To model the PEMWE single-cell, COMSOL Multiphysics was used by coupling a three-dimensional geometric model with multi-physics fields such as electrochemical kinetics, mass transfer, and heat transfer. The developed PEMWE single-cell three-dimensional geometric model is illustrated in Fig. 2.

Electrochemical kinetics

The operating voltage of a PEMWE single-cell consists of open-circuit voltage V_{oc}, activation overpotential V_{act}, concentration overpotential V_{con}, and ohmic overpotential V_{ohm}, expressed by Ref. [41]:

$$V_{cell} = V_{oc} + V_{act} + V_{con} + V_{ohm} \quad (3)$$

Here, V_{oc} is calculated using the Nernst equation:

$$V_{oc} = E_0 + \frac{RT}{2F}\left[\ln\left(\frac{p_{H_2}\sqrt{p_{O_2}}}{a_{H_2O}}\right)\right] \quad (4)$$

where R represents the universal gas constant, F is the Faraday constant, T denotes the operating temperature, p_{H2} and p_{O2} are the partial pressures of hydrogen and oxygen and a_{H2O} is the water activity between electrode and membrane (1 for liquid water). Furthermore, E_0 represents the standard electric potential of the electrolyzer. In the literature, E_0 is commonly assumed to be 1.23 V, but it can be affected by the operating temperature. In this work, we adopt the following equation [42]:

$$E_0 = 1.229 - 0.9 \times 10^{-3}(T - 298) \quad (5)$$

In Eq. (3), V_{act} is caused by the slowness of the electrode reaction kinetics. Using the Butler-Volmer equation for the electrode surface reaction, V_{act} can be expressed in terms of current density as follows:

$$i = i_0\left[\exp\left(\frac{\alpha_{an}FV_{act}}{RT}\right) - \exp\left(-\frac{\alpha_{cat}FV_{act}}{RT}\right)\right] \quad (6)$$

where i denotes the current density, i_0 represents the exchange current density, and α_{an} and α_{cat} are the anode and cathode charge transfer coefficients, respectively. Based on Eq. (6), we have

$$V_{act} = \frac{RT}{\alpha_{an}F}\operatorname{arcsinh}\left(\frac{i}{2i_{an,0}}\right) + \frac{RT}{\alpha_{cat}F}\operatorname{arcsinh}\left(\frac{i}{2i_{cat,0}}\right) \quad (7)$$

Since the reactants on the surface of the porous electrode are consumed, the electrode surface will produce a concentration difference from the solution itself. The reactants will slowly diffuse to the active site, causing a loss of electrolyzer voltage. Therefore, V_{con} is essentially the external manifestation of particle diffusion. Combining the Nernst equation with Fick's law, the expression of V_{con} is given as follows:

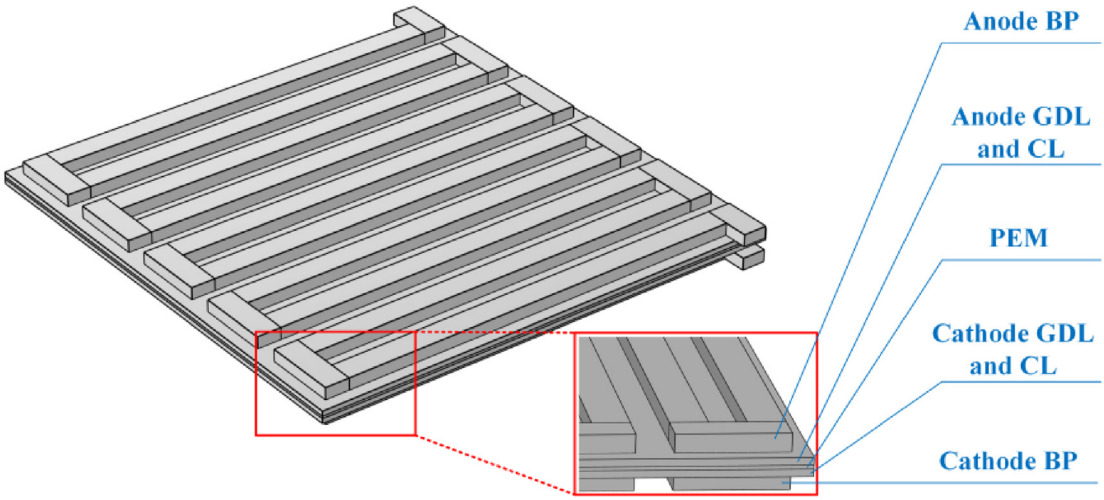

Fig. 2 – PEMWE single-cell three-dimensional geometric model.

$$V_{con}=\frac{RT}{4F}\ln\left(\frac{c_{O_2}}{c_{O_2,0}}\right)+\frac{RT}{2F}\ln\left(\frac{c_{H_2}}{c_{H_2,0}}\right) \tag{8}$$

where c_{O2} and c_{H2} denote the concentrations of oxygen and hydrogen at the intersection of membrane and electrode, respectively, and $c_{O2,0}$ and $c_{H2,0}$ denote the corresponding reference values.

Ohmic polarization arises from the resistance to ion flow and the equivalent resistance present in the electrodes and the bipolar plate itself. According to Ohm's law, the V_{ohm} appears to be linearly proportional to the electrolytic current during electrolysis, as shown in the following equation:

$$V_{ohm}=(2R_{BP}+2R_{GDL}+2R_{CL}+R_{in})iA \tag{9}$$

where A is the activated membrane area. The ohmic resistance of BP and GDL is calculated from the material resistivity. The ohmic resistance of CL is generally ignored since the CL is very thin. Furthermore, R_{in} represents the resistance of the ion in passing through the membrane and it is given by Ref. [43]:

$$\begin{cases} R_{in}=\dfrac{\delta_{PEM}}{\sigma_{PEM}} \\ \sigma_{PEM}=(0.005139\lambda-0.00326)\exp\left[1268\left(\dfrac{1}{303}-\dfrac{1}{T}\right)\right] \end{cases} \tag{10}$$

where δ_{PEM}, σ_{PEM}, and λ denote the thickness, conductivity, and water content of PEM, respectively.

Mass transfer

Mass and momentum conservation equations are used to describe the mass transfer of the mixture within the PEMWE single-cell [44]:

$$\begin{cases} \nabla\cdot(\varepsilon\rho_f v)=0 \\ \nabla\cdot(\varepsilon\rho_f v^2)=-\varepsilon\nabla p+\nabla\cdot(\varepsilon\mu v)+S_v \end{cases} \tag{11}$$

where ε represents the porosity of the porous medium, μ and ρ_f are the viscosity and average density of the fluid mixture, respectively, S_v denotes the source term, p represents the operating pressure, and v is the volume average velocity of the fluid mixture [45].

Convection and diffusion of each component of the gas-liquid flow in the porous medium are described by the Maxwell-Stefan equation:

$$\nabla\cdot(\varepsilon v_m c_m)=\nabla\cdot\left(\varepsilon^{1.5}d_m\nabla c_m\right)+s_m \tag{12}$$

where s_m is the mass source term of the m-th material phase, v_m, c_m and d_m are the volume average velocity, molar concentration material and the effective diffusion coefficient of the m-th material phase, and d_m is the function of temperature and pressure:

$$d_m=d_{m,0}\left(\frac{T}{T_0}\right)^{1.5}\left(\frac{p_0}{p}\right) \tag{13}$$

where $D_{m,0}$ is the diffusion coefficient of the binary component, T_0 and p_0 denote the T and p reference value.

Heat transfer

Electrochemical reactions and heat generation and consumption occur simultaneously during the operation of the PEMWE. While the electrolysis of water is typically an endothermic process, in electrolysis cells, significant heat might be generated. Thus, compared to other types of electrolyzers, the PEMWE is more complicated in terms of heat transmission. An electrolysis cell's thermal equilibrium can be described by its energy equation:

$$\nabla\cdot\left(\rho_{eff}C_{eff}\vec{v}_m\right)T=\nabla\cdot\left(\gamma_{eff}\nabla T\right)+S_T \tag{14}$$

where ρ_{eff}, C_{eff}, and γ_{eff} are the effective average density, effective heat capacity, and effective thermal conductivity, respectively, given by:

$$\begin{cases} \rho_{eff}=(1-\varepsilon)\rho_s+\varepsilon\rho_f \\ C_{eff}=(1-\varepsilon)C_s+\varepsilon C_f \\ \gamma_{eff}=(1-\varepsilon)\gamma_s+\varepsilon\gamma_f \end{cases} \tag{15}$$

where ρ_s, C_s, and γ_s represent the average density, heat capacity, and thermal conductivity of the solid areas, respectively. ρ_f, C_f, and γ_f represent the average density, heat capacity, and thermal conductivity of the fluid mixture,

Table 1 – Parameters of PEMWE single-cell model.

Names	Parameters	Value	Unit
Faraday constant	F	96,486	C/mol
Universal gas constant	R	8.314	J/(mol K)
Activated membrane area	A	4	cm^2
PEM thickness	δ_{mem}	100	μm
Anode/Cathode thickness	δ_{an}/δ_{cat}	200	μm
Anode transfer coefficient	α_{an}	0.5	–
Cathode transfer coefficient	α_{cat}	0.5	–
Exchange current density at anode	$i_{an,0}$	1×10^{-8}	A/cm^2
Exchange current density at cathode	$i_{ca,0}$	1×10^{-3}	A/cm^2
PEM conductivity	σ_{PEM}	10	S/m
GDL conductivity	σ_{GDL}	530	S/m
PEM porosity	ε_{PEM}	0.5	–
GDL porosity	ε_{GDL}	0.77	–
Thermal conductivity of PEM	γ_{PEM}	0.67	W/(m K)
Thermal conductivity of GDL	γ_{GDL}	15.2	W/(m K)
Thermal conductivity of H_2	γ_{H2}	0.204	W/(m K)
Thermal conductivity of O_2	γ_{O2}	0.0296	W/(m K)
Operating pressure	p	10	kPa
Operating temperature	T	353	K
Current density range	i	0–3	A/cm^2
Voltage range	V_{cell}	1.49–2.02	V

respectively. Furthermore, S_T in Eq. (14) is the source term that can be calculated from the study by Toghyani [46] et al.

The parameters of the PEMWE single-cell model used in this work are given in Table 1 [46–49].

From the simulation of the PEMWE single-cell model, the operating voltage $V_{cell} = 1.8286$ V is obtained when the current density $i = 1$ A/cm^2. Fig. 3 illustrates the molar fractions of water and oxygen at the anode. It can be seen that as the oxidation reaction proceeds, the water content in the electrolyzer gradually decreases and the oxygen content gradually increases. The oxygen concentration is the largest and the water content is the lowest at the exit of the anode flow field.

The polarization curve of the PEMWE single-cell is shown in Fig. 4. With the increase of current density, the operating voltage V_{cell} rises from near the thermoneutral voltage V_{th} to $V_{cell} = 2.02$ V at $i = 3$ A/cm^2. The voltage increases very fast at low currents and it gradually slows down, showing a non-linear rising trend. It can be seen that V_{ohm} dominates this trend, verifying the model's accuracy.

Efficiency and degradation analysis of PEMWE

The efficiency of PEMWE using external electrical energy is generally expressed by the voltage efficiency η_V, which reflects the membrane loss and heat loss. It is defined as the ratio of V_{th} to V_{cell} [13]:

$$\eta_V = \frac{V_{th}}{V_{cell}} \tag{16}$$

Based on the single-cell polarization curve as shown in Fig. 4 and Eq. (16), we can compute η_V at different current densities. Since this efficiency term is close to 100% at low current densities, it cannot fully reflect the electrolyzer efficiency η_{el}. η_{el} can be expressed as the product of η_V, Faraday efficiency η_F and auxiliary equipment efficiency η_{ae}:

$$\eta_{el} = \eta_V \cdot \eta_F \cdot \eta_{ae} \tag{17}$$

where η_F reflects losses caused by gas diffusion and is closely related to operating pressure p, given by Refs. [50–52]. And auxiliary equipment generally refers to electrolyzer water and heat management equipment, with the efficiency around 90%.

$$\eta_F = (-0.0034p - 0.001711) \cdot i^{-1} + 1 \tag{18}$$

The relationship between PEMWE single-cell and single-stack is shown in Eq. (19). The parameters of the 60-kW PEMWE used in this work are shown in Table 2, which are based on the simulation results and existing commercial PEMWE parameters.

$$\begin{cases} P_{el} = V_{el} \cdot I_{el} \\ V_{el} = n_{el} \cdot V_{cell} \\ I_{el} = i \cdot A \end{cases} \tag{19}$$

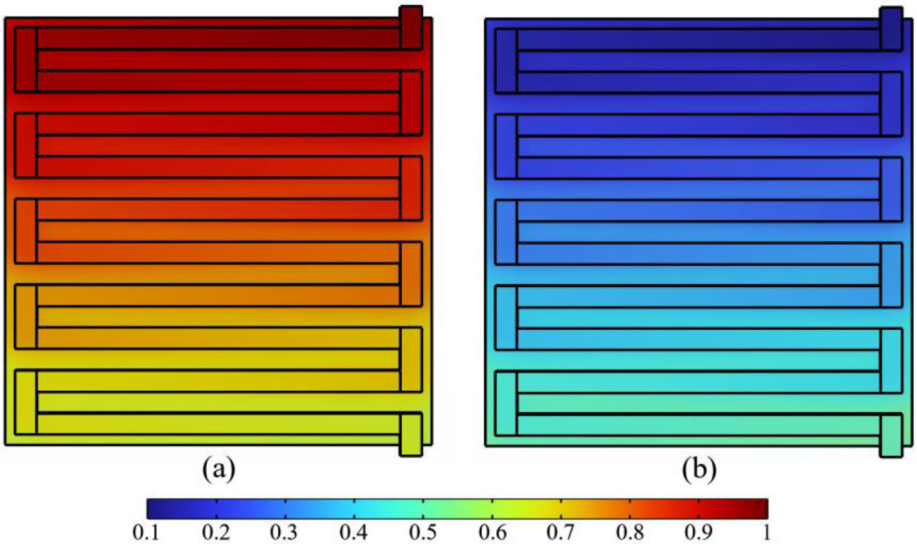

Fig. 3 – Anode molar fractions of (a) water and (b) oxygen.

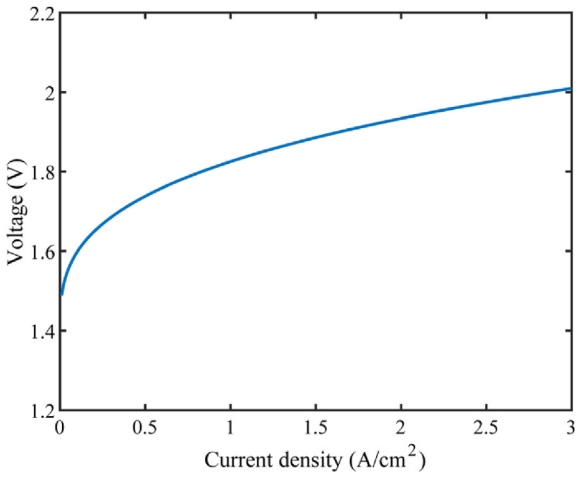

Fig. 4 – Polarization curve of PEMWE single-cell.

Table 2 – Parameters of a 60-kW PEMWE.

Names	Parameters	Value	Unit
Rated power	P_{el}	60	kW
Operating voltage	V_{el}	75–100	V
Operating current	I_{el}	8–600	A
Cells number	n_{el}	50	–
Activated membrane area	A	200	cm^2
Operating pressure	p	10	kPa
Operating temperature	T	353	K

Based on Eqs. (16)–(19) and Table 2, Fig. 5 shows the simulated relationship between efficiency and power of 60-kW PEMWE. When the input power is less than 600 W, V_{el} is too low for the PEMWE to perform hydrogen production. This is consistent with the experimental results of Weiss [26] et al. At low power ranges, η_{el} increases rapidly with increasing current density. It reaches its maximum value of 71.57% when at $P_{el} = 9.41$ kW, and then slowly decreases. In this process, η_F dominates in the low power range, while in the medium and high power ranges, η_F approaches 100%, and thus the total efficiency is mainly determined by η_V.

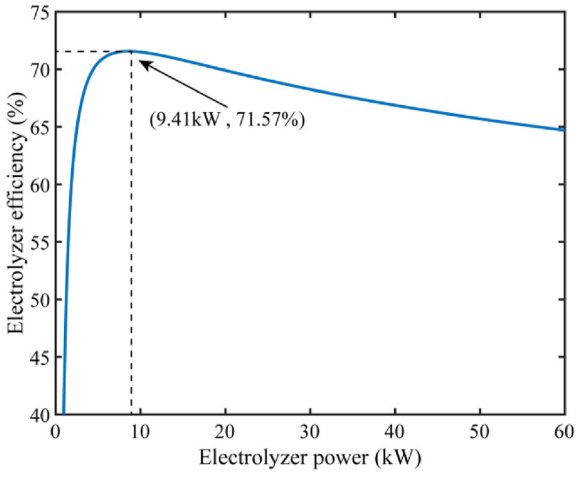

Fig. 5 – Relationship of efficiency versus power of a 60-kW PEMWE.

Table 3 – Degradation of PEMWE components under dynamic operation.

Degradation modes	Causes	Consequences
Dissolution of catalyst	High operating potential; Current reversal during power off	$V_{act}\uparrow$
Agglomeration of catalyst	Load cycle and start-stop switching; High current density	$V_{act}\uparrow$ $V_{ohm}\uparrow$
Passivation of catalyst support	High operating potential	$V_{con}\uparrow$ $V_{ohm}\uparrow$
Passivation of electrode	High current density; Frequent fluctuations of current	$V_{ohm}\uparrow$
Dissolution of membrane	High current density	$V_{ohm}\downarrow$
Poisoning of membrane	Load cycle and start-stop switching; Frequent fluctuations of current	$V_{con}\uparrow$ $V_{ohm}\uparrow$

Dynamic operation is an important cause of PEMWE degradation, and the degradation of PEMWE will cause a rise in the operating voltage. The main causes of the degradation of different components of the PEMWE are summarized in Table 3 [22–24,26,28,53]. With the development of AST, researchers have proposed that the voltage degradation rate of PEMWE varies under different operating conditions, and the voltage degradation rate can be used to quantitatively characterize the degree of degradation of PEMWE. Low and medium constant input power has little effect on voltage degradation rate. However, frequent start-stop switching and high constant input power have a great impact on the voltage degradation rate, up to 230 μV/h; Additionally, fluctuating operation within the rated power of the PEMWE is beneficial in the short term to slow down aging, but the opposite is true in the long term, even more, severe voltage degradation caused by high power fluctuation operation [12,54,55].

When the V_{cell} gradually increases with the degradation of PEMWE, the η_V will decrease and the efficiency of PEMWE at the same power will gradually decrease, as shown in Fig. 6. In a large-scale wind-hydrogen system, due to the small power level of PEMWE single-stack, multiple electrolyzers need to be combined to produce hydrogen. By optimizing the power allocation of the multi-stack PEMWE array in the wind-hydrogen system, it will not only extend the PEMWE lifetime but also improve the overall system energy efficiency.

Optimization of power allocation

Conventional power allocation strategy

The conventional power allocation strategies are mainly divided into average allocation strategy and daisy chain allocation strategy. The average allocation strategy means that a constant number of electrolyzers are put into operation and

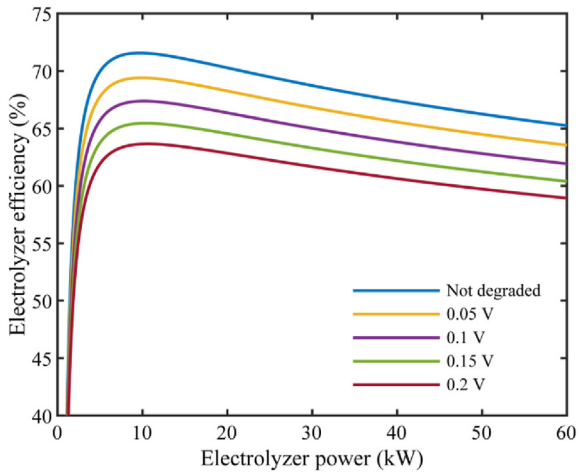

Fig. 6 – Efficiency of PEMWE at different voltage degradation.

the system input power is allocated equally to each single-stack. In the daisy chain allocation strategy, single-stacks are put into operation one by one, with the previous electrolyzer reaching rated power before starting the next one, and so on. Some researchers have studied the power allocation strategy considering optimal efficiency, when the system efficiency using k+1 electrolyzers is equal to the system efficiency using k electrolyzers, the corresponding power is denoted as the start-stop power point P_k. When the system input power is larger than P_k, the input power is equally allocated by k+1 electrolyzers. Otherwise, the input power is allocated equally by k electrolyzers. Taking a multi-stack system consisting of four 60-kW PEMWE single-stacks as an example, the variation of system efficiency with input power under three power allocation strategies is shown in Fig. 7.

It can be seen from Fig. 7 that compared to the daisy chain strategy, the average allocation strategy is more efficient in the middle and high power ranges but less efficient in the low power range. When the input power is wind power, the average allocation strategy will result in all electrolyzers

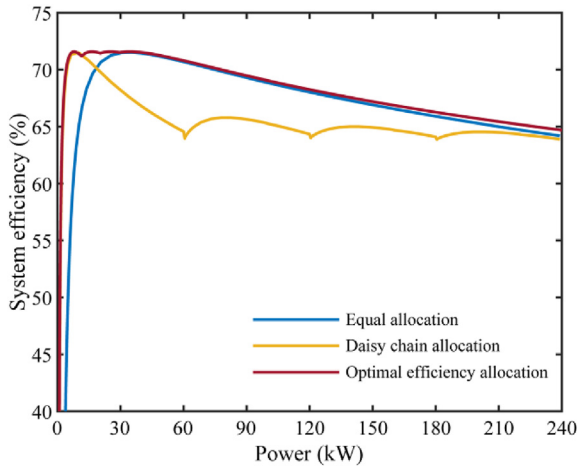

Fig. 7 – Variation of system efficiency with input power under three power allocation strategies.

bearing the same wind power fluctuation together, and the first electrolyzer to start in the daisy chain allocation strategy will operate in the high power range for a long time. Although the power allocation strategy considering optimal efficiency ensures that the system efficiency is always optimal, P_k is almost always in the low power range. Each electrolyzer still faces the problem of frequent start-stop switching, which will be more serious during low wind speed periods. At the same time, in order to ensure optimal efficiency at all times, this strategy requires an equal allocation of system input power after determining the number of electrolyzers in operation. This results in the need to instantaneously increase the power from zero to the allocated value for an electrolyzer that has just been started up, which is difficult to achieve in real-world applications.

A proposed power allocation strategy considering degradation conditions

The connection methods of multi-stack electrolyzer or fuel cell array are mainly divided into series architecture, parallel architecture, series-parallel architecture and cascade architecture [30]. In the series architecture, each single-stack cannot be controlled individually and without a bypass circuit, the failure of one stack leads to the failure of the entire system. In the parallel architecture, each single-stack is powered by a corresponding converter, allowing for complete independent control, but also resulting in higher costs. Series-parallel architecture and cascade architecture combine both parallel and series architecture, this configuration balances both the advantages and the drawbacks of each configuration. However, they still cannot realize the completely independent control of each single-stack, which hinders the implementation of power allocation strategy, so this paper adopts parallel architecture.

An overview of the basic architecture of the wind-hydrogen system is shown in Fig. 8. The input wind power P_{wind} is connected to the multi-stack PEMWE array (in parallel) through a DC bus, and the power allocation is divided into the control module and the execution module. The control module collects data on the operation of each PEMWE single-stack and sends the power allocation signal to the execution module in time. In addition, the control module controls the start-stop of the external power supply to each PEMWE single-stack to maintain the operation of the electrolyzer in the absence of wind power input. The execution module consists of extended duty cycle interleaved buck converter (EDCIBC) based on a fuzzy PID control which supplies power to each single-stack, adjusting the input power of each PEMWE single-stack according to the received power allocation signal.

Control module

First, the allocation module needs to determine a turning power point P_t to split the operating power range. For a system PEMWE with K single-stacks, when $P_{wind} < (K \cdot P_t)$, all single-stacks will operate under the daisy chain allocation strategy. The (k+1)th single-stack is put into operation when the kth single-stack operating power reaches the P_t. When $P_{wind} > (K \cdot P_t)$, the excessive power will be equally allocated to each single-stack.

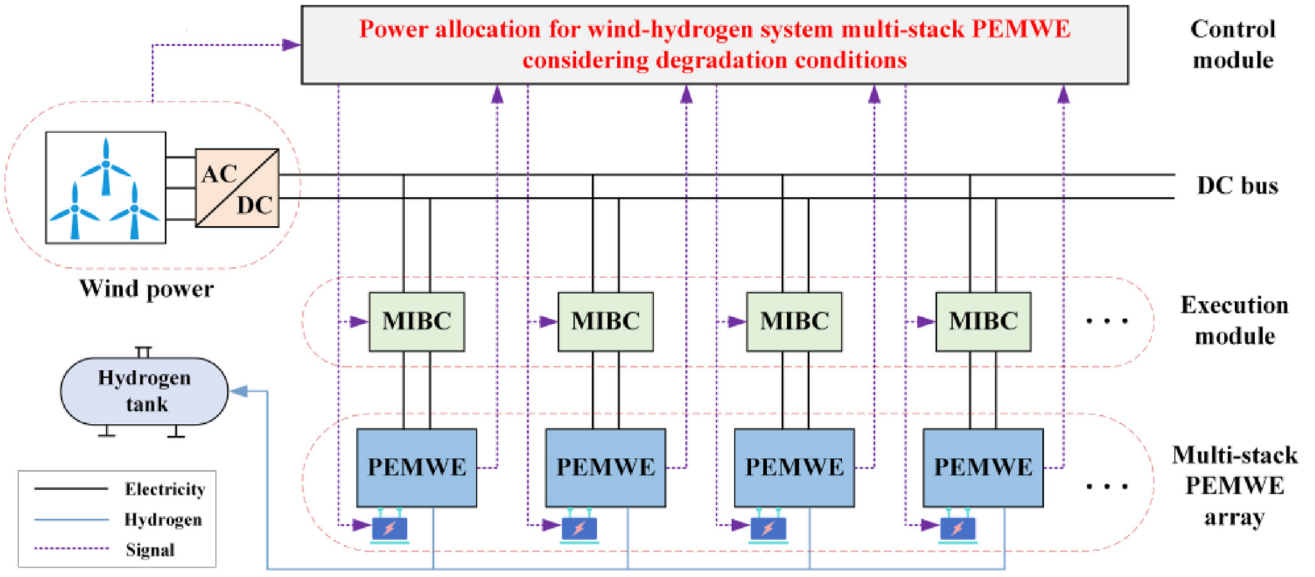

Fig. 8 – Basic architecture of the wind-hydrogen system.

In addition, the PEMWE cannot be restarted immediately when it is fully stopped. Hence it cannot be used to cope with high fluctuation of input wind power. And frequent start-stop switching also causes hydrogen to collect at the anode and permeate through the membrane to the cathode, leading to severe safety problems. Some studies suggest using low power supplies to maintain the voltage of the electrolyzer when there is no electrical input [25,26]. In the power allocation strategy proposed in this work, a 600 W external power supply is applied to maintain the PEMWE operating at the minimum operating voltage when no sufficient wind power is available for hydrogen generation.

Based on the voltage degradation rates under different operating conditions concluded from the current study, we divide the PEMWE operations into five conditions: maintenance operation, low power fluctuation operation, constant turning power operation, high power fluctuation operation, and constant rated power operation. The power range and PEMWE single-cell voltage degradation rate for each operating condition are shown in Table 4. In commercial PEMWE products, the current density over 2 A/cm^2 is generally identified as high power operation. Thus, the turning power point P_t of the 60-kW PEMWE used in this work is assumed to be 40 kW.

Table 4 – Power range and PEMWE single-cell voltage degradation rate for five operating conditions.

Operating conditions	Parameters	Power range (kW)	Voltage degradation rate (μV/h)
Maintaining operation	V_m	0.6	1.5
Low power fluctuation operation	V_{fl}	(0.6,P_t)	50
Constant turning power operation	V_{ct}	P_t	20
High power fluctuation operation	V_{fh}	(P_t,P_{el})	66
Constant rated power operation	V_{cr}	P_{el}	196

We assume that the voltage degradation rates under different operating conditions are independent of each other, and the performances of all cells within the same PEMWE single-stack are the same. Thus, the total voltage degradation of the PEMWE single-stack can be expressed as:

$$\Delta V_d = n_{el} \cdot (t_m \cdot V_m + t_{fl} \cdot V_{fl} + t_{ct} \cdot V_{ct} + t_{fh} \cdot V_{fh} + t_{cr} \cdot V_{cr}) \quad (20)$$

where t_m, t_{fl}, t_{ct}, t_{fh}, and t_{cr} are the operating times under the corresponding operating conditions, respectively.

When the wind-hydrogen system requires to operate with multiple PEMWE single-stacks, allocating the power in a fixed order will lead to longer operation time and more serious

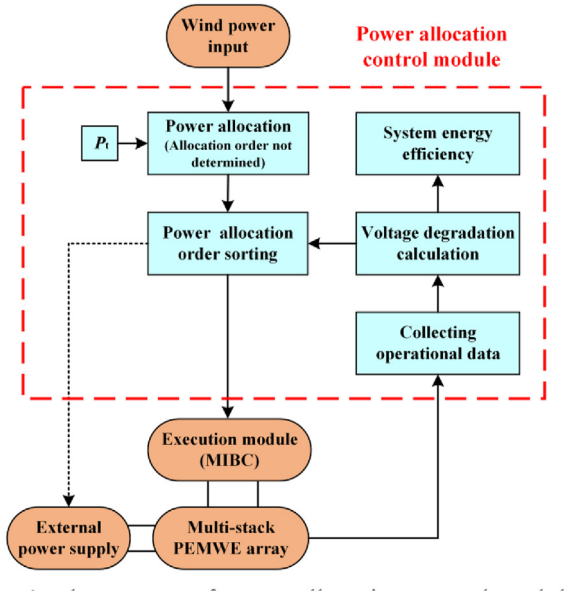

Fig. 9 – The process of power allocation control module.

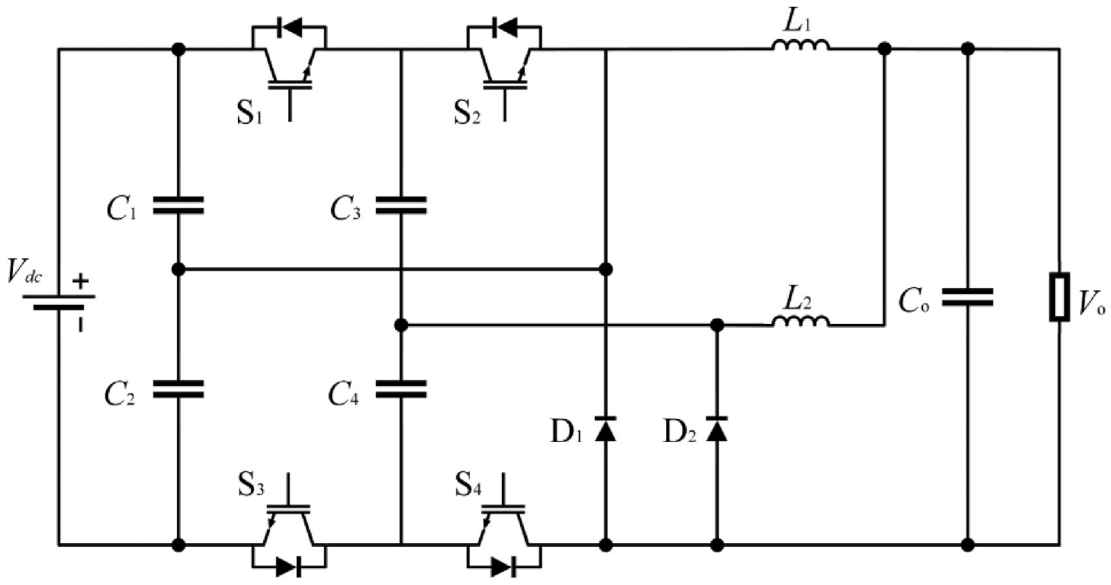

Fig. 10 – Extended duty cycle interleaved buck converter (EDCIBC).

voltage degradation for the single-stack that is allocated earlier. This will result in performance inconsistency for different single-stacks. Therefore, the power allocation order needs to take into account the voltage degradation status of each PEMWE single-stack. If a PEMWE single-stack needs to be put into operation, one should first prioritize using the one with the least degradation. On the other hand, the most degraded stack should be selected when a stack is required to be stopped.

As shown in Fig. 9, the power allocation control module mainly consists of operational data acquisition and online calculation. With the wind power input, the control system first determines the number of PEMWE single-stacks that will be put into operation and the power allocated to each single-stack. At the same time, the operating conditions of each PEMWE single-stack are collected, and the power allocation order of each single-stack is determined by an online calculation of the voltage degradation. If a single-stack has no wind power input, its external power supply is used to maintain its operation. Additionally, the system updates each single-stack efficiency curve based on the voltage degradation status and monitors the external power supply operating time to calculate the system energy efficiency.

Execution module

According to Faraday's law, the hydrogen production rate of a PEMWE single-cell is proportional to the electron transfer rate on the electrodes, which equals the external circuit current. Thus, the total hydrogen production rate of a PEMWE single-stack consisting of multiple PEMWE single-cells in series is as follows:

$$N_{H_2} = \eta_F \cdot \frac{n_{el} I_{el}}{2F} \tag{21}$$

As can be seen from Eq. (21), the size and quality of the electrolysis current will directly affect hydrogen production. In addition, current ripple Δi_o from the converter harms the life of the PEM fuel cell and electrolyzer, and high-frequency current ripples will lead to more severe degradation [36,56]. Therefore, the output current ripple of the converter of each PEMWE

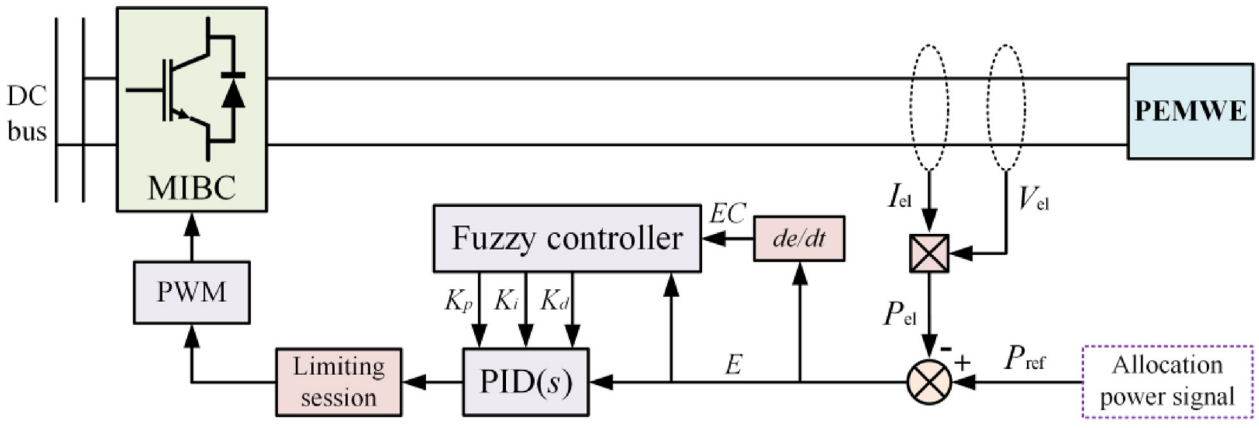

Fig. 11 – EDCIBC based on fuzzy PID control.

Table 5 – Fuzzy control rules of K_p, K_i and K_d.

K_p		E						
		NB	NM	NS	ZO	PS	PM	PB
EC	NB	PB	PB	PB	ZO	NB	NM	ZO
	NM	PB	PB	PM	ZO	NM	PS	PS
	NS	PB	PM	PS	ZO	ZO	PM	PM
	ZO	PM	PS	PS	ZO	PS	PM	PB
	PS	PS	PS	ZO	ZO	PS	PM	PS
	PM	ZO	ZO	NS	ZO	PM	PB	PB
	PB	ZO	NS	NM	ZO	PM	PB	PB
K_i		E						
		NB	NM	NS	ZO	PS	PM	PB
EC	NB	NB	NB	NM	NM	NS	NS	ZO
	NM	NB	NB	NM	NS	NS	ZO	ZO
	NS	NM	NM	NM	ZO	ZO	PS	PS
	ZO	NM	NS	NS	ZO	PS	PS	PM
	PS	NS	NS	ZO	PS	PS	PM	PB
	PM	ZO	ZO	PS	PS	PM	PB	PB
	PB	ZO	ZO	PS	PM	PM	PB	PB
K_d		E						
		NB	NM	NS	ZO	PS	PM	PB
EC	NB	PM	NS	NB	NB	NM	NM	PS
	NM	PS	NM	NB	NM	NM	NM	ZO
	NS	PS	NM	NM	NM	NS	NS	ZO
	ZO	ZO	NS	NS	NS	NS	NS	ZO
	PS	ZO	NS	ZO	ZO	ZO	ZO	ZO
	PM	PM	ZO	PS	PS	PS	PS	PB
	PB	PB	PM	PM	PM	PS	PS	PB

single-stack should be maintained as small as possible, so that low-voltage high-current outputs can be achieved.

As shown in Fig. 10, we adopt the EDCIBC proposed in Ref. [37], since it can achieve the above requirements. The EDCIBC is obtained by adding four capacitors C_1, C_2, C_3, and C_4 to the conventional two-phase interleaved parallel buck converter. Based on the principle of capacitive voltage division, the EDCIBC can store energy in the input capacitors to improve the voltage ratio R and reduce the voltage stress of the switching device V_S. The static characteristics of EDCIBC are as follows:

$$R = \frac{V_o}{V_{dc}} = \frac{D}{4} \tag{22}$$

$$\Delta i_o = \frac{(1-2D)DV_{dc}}{4Lf_s} \tag{23}$$

$$\begin{cases} V_{S1} = V_{S2} = V_{S3} = \dfrac{V_{dc}}{2} \\ V_{S4} = \dfrac{V_{dc}}{4} \end{cases} \tag{24}$$

where V_o is the output voltage, V_{dc} is the input voltage, D is the duty cycle of the switching device, L is the output inductor ($L_1 = L_2 = L$ in Fig. 10), and f_s is the switching frequency of the switching device.

Theoretically, the Δi_o of EDCIBC is significantly reduced compared to the conventional buck converter, and a high voltage ratio can be obtained without using a small duty cycle. V_S is not higher than one-half of the input voltage, and V_{S4} is only one-fourth of the input voltage. Meanwhile, from the experiments of Pan et al. the average efficiency of EDCIBC is around 94%, and the major losses come from the active switches, the diodes, and the output inductors. When replaced with lower loss switching devices, the EDCIBC will achieve an efficiency of 96%, which is considered ideal in the analysis below. Therefore, the static characteristics of EDCIBC fit the requirements for renewable energy hydrogen production applications.

When the EDCIBC is connected to a linear load, the control requirements can be fulfilled by using conventional PID control; however, when the load is a non-linear load such as PEMWE, using fixed values of K_p, K_i and K_d will not fulfill the

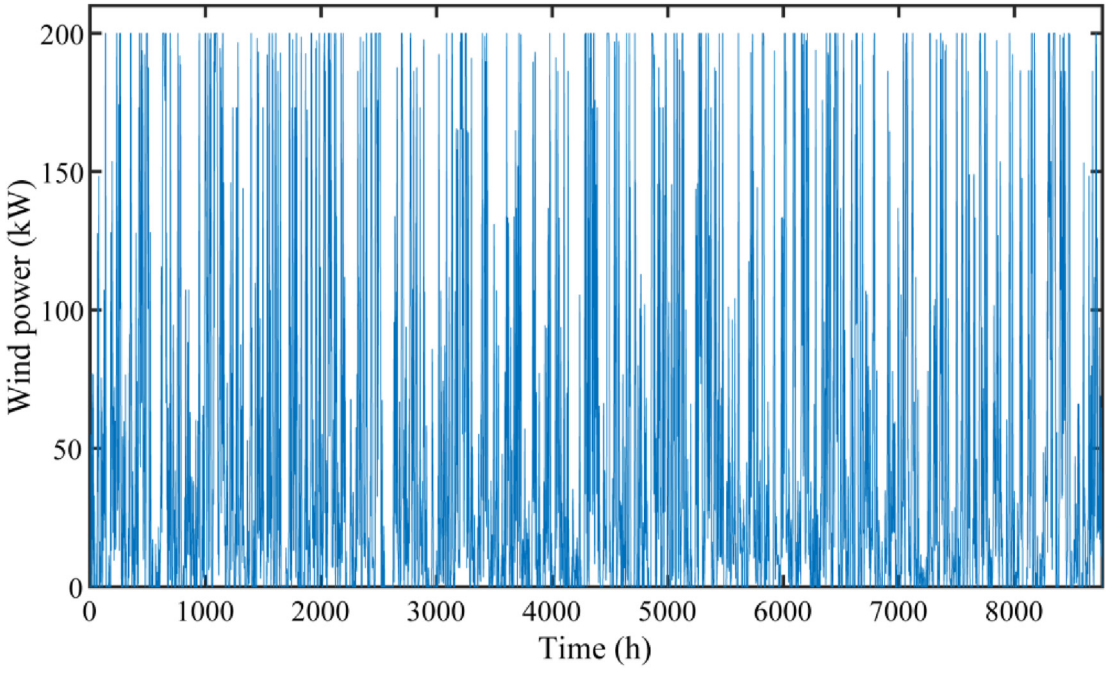

Fig. 12 – Annual (8760 h) output power of a 200-kW wind turbine.

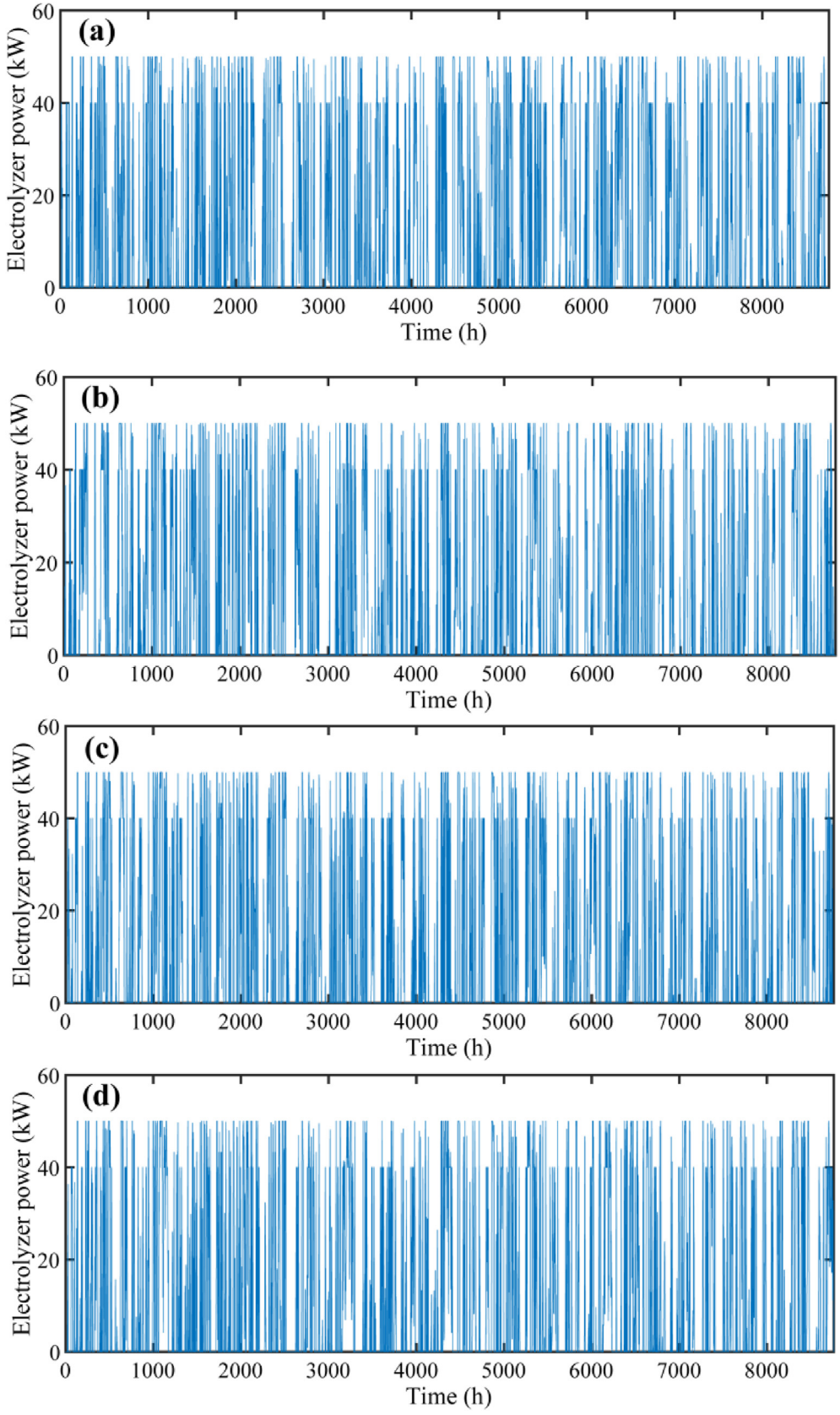

Fig. 13 – Operating power of four PEMWE single-stack in 8760 h. (a) PEMWE 1. (b) PEMWE 2. (c) PEMWE 3. (d) PEMWE 4.

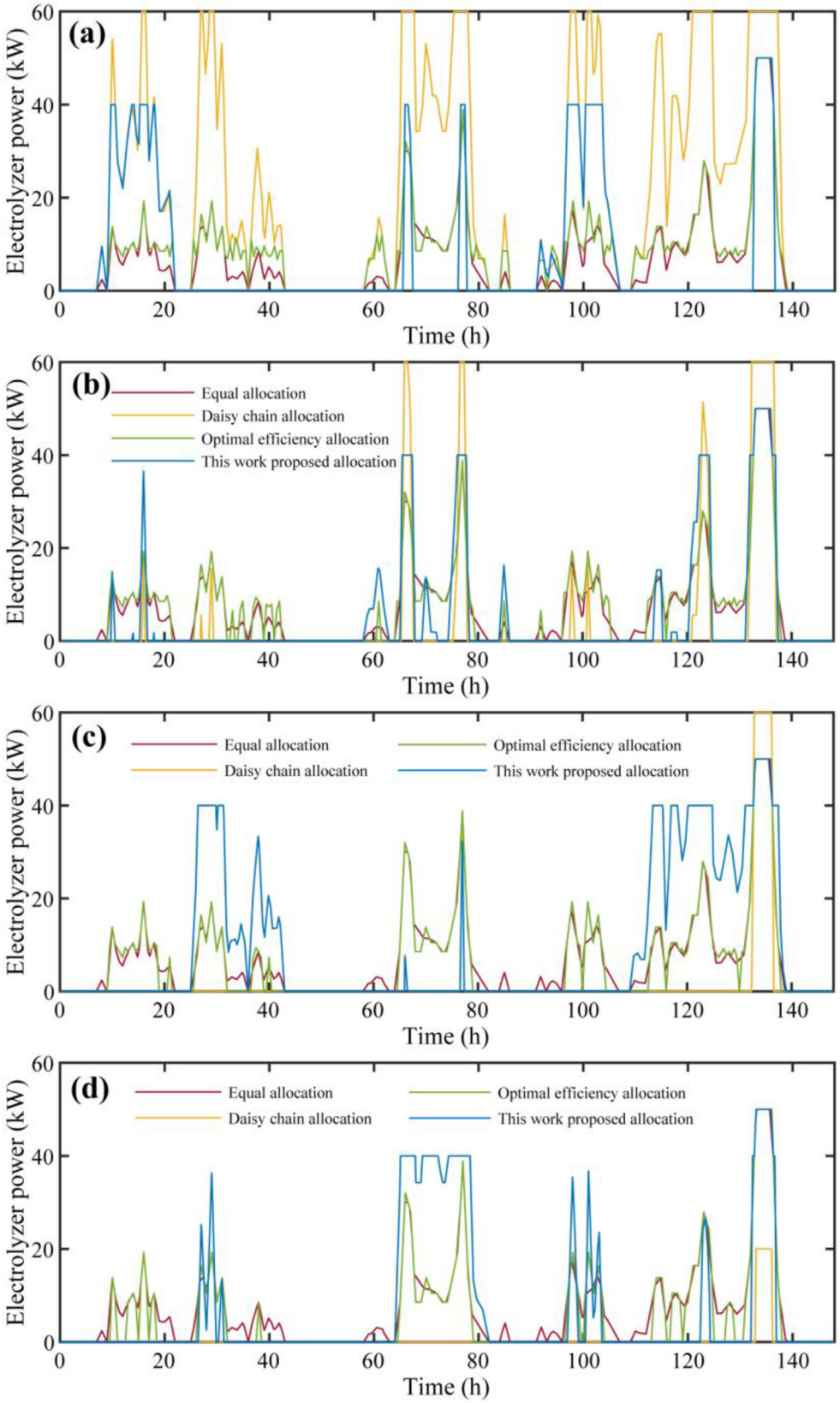

Fig. 14 – Operation of each PEMWE single-stack for the first 148 h under different power allocation strategies. (a) PEMWE 1. (b) PEMWE 2. (c) PEMWE 3. (d) PEMWE 4.

requirements of the EDCIBC for fast signal following, its control accuracy is relatively low. Parameter adjustment of PID controller using artificial intelligence algorithm is an improved idea, artificial intelligence-based controls can achieve fast response, small overshoot and fast convergence, However, they are relatively difficult to be implemented in practice due to their high dependence on a large amount of data and high complexity [57]. In practical projects, fuzzy logic control is preferred for the control of converters. The advantages of fuzzy logic control are timely response and simple structure, meanwhile, it does not require a complex model and closely combines with PID control, which can achieve high control accuracy by simply constructing suitable fuzzy control rules [58]. Therefore, the fuzzy controller is added on the basis of PID control to form EDCIBC based on fuzzy PID control, as shown in Fig. 11.

The fuzzy controller adopts the structure of two inputs and three outputs. The difference E between the actual operating power of the PEMWE single-stack and the power allocated by the system, and the change rate EC of the E are the input. The dynamic PID parameters K_p, K_i, and K_d are calculated by the fuzzy controller and output to the PID controller to complete the control. In the fuzzy controller, the E is divided into seven levels: NB (Negative big), NM (Negative medium), NS (Negative small), Z (Zero), PS (Positive small), PM (Positive medium), and PB (Positive big). PB represents that the actual operating power of PEMWE is much less than the system allocated power, and NB represents that the actual operating power is much bigger than the system allocated power. The fuzzy control rules of K_p, K_i, and K_d are shown in Table 5. In addition, the degree of membership function selects the triangle function and the method of defuzzification selects the center-of-gravity method.

Simulation results and discussions

Verification of power allocation control module

A hydrogen-electric coupled DC microgrid demonstration project was established in 2020 in Cixi City, Zhejiang Province, China. The annual (8760 h) output power data of a 200-kW wind turbine in this project is shown in Fig. 12. The wind at this location is highly fluctuating, so the wind turbine rarely operates at rated power and is frequently shut down at low wind periods. Based on the wind turbine output, a multi-stack array consisting of four 60-kW PEMWE single-stacks (denoted by PEMWE 1 to PEMWE 4) is used in the wind-hydrogen system. The measured operating power of each PEMWE single-stack in 8760 h is shown in Fig. 13. It can be seen that each

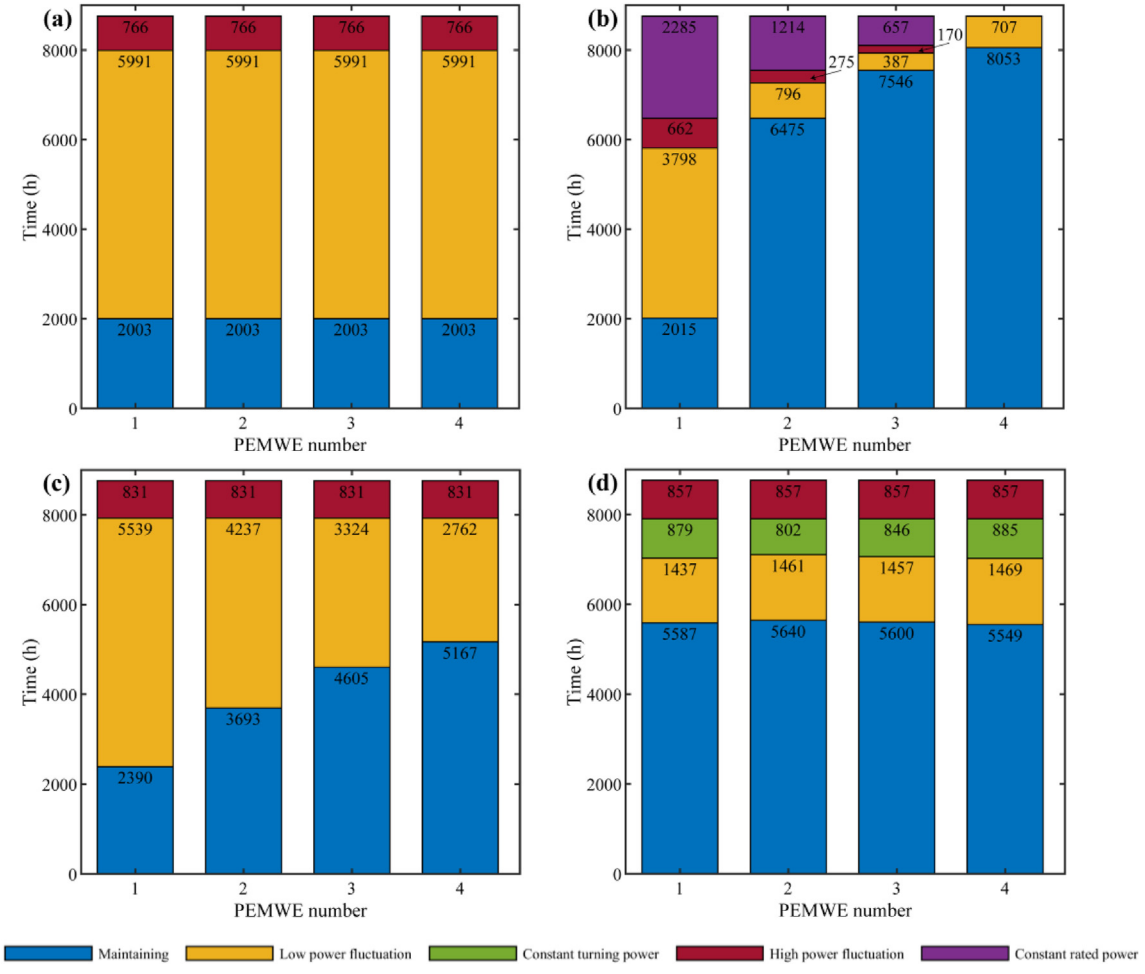

Fig. 15 – The operating time of each PEMWE single-stack under five operating conditions with (a) average allocation, (b) daisy chain allocation, (c) optimal efficiency allocation, and (d) proposed allocation strategy.

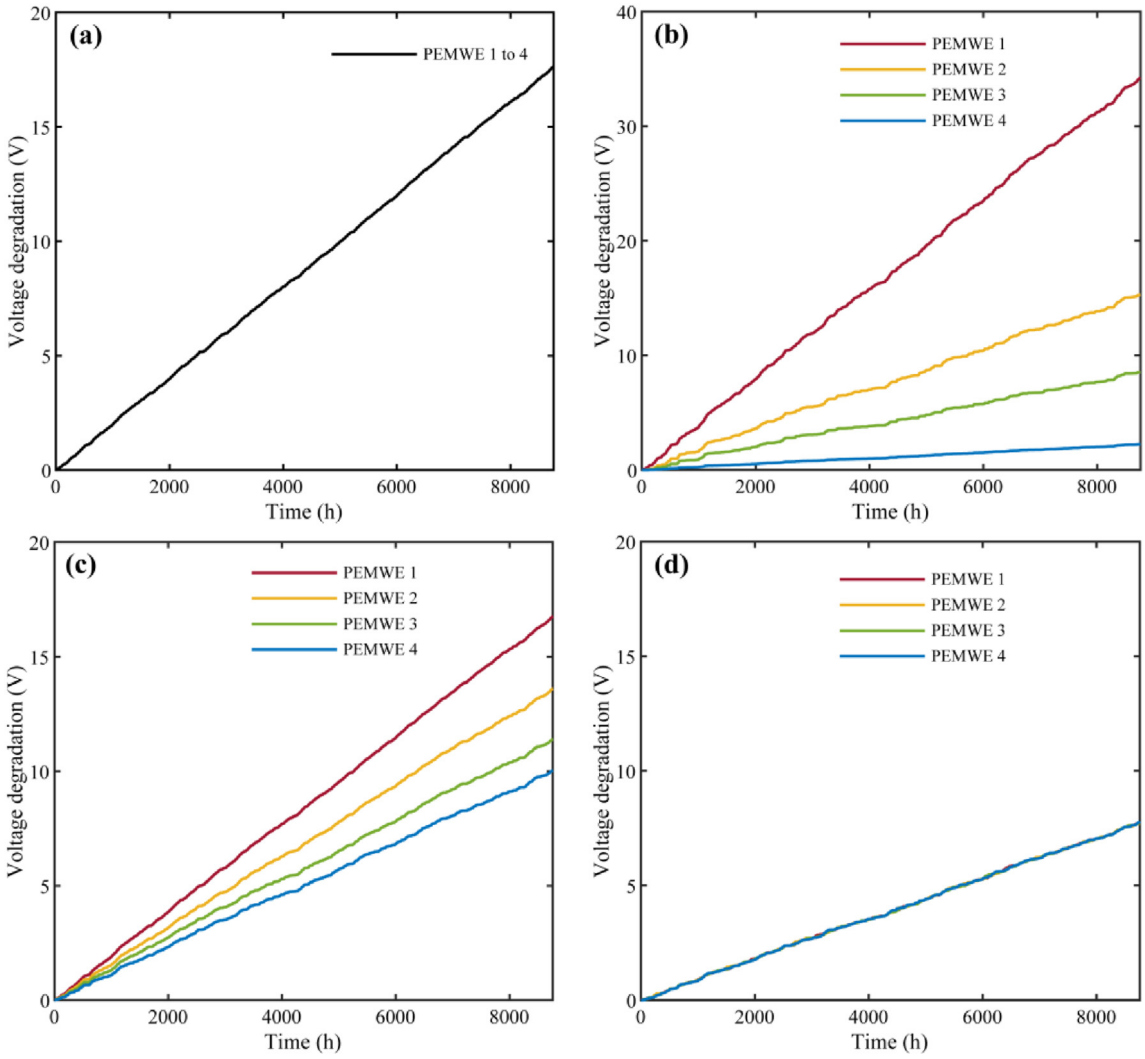

Fig. 16 – The voltage degradation of each PEMWE single-stack under (a) average allocation, (b) daisy chain allocation, (c) optimal efficiency allocation, and (d) proposed allocation strategy.

single-stack operates at similar operating conditions and operates below the P_t most of the time without over-operation or long-time idle.

To clearly compare the power allocation of each single-stack under different strategies, the operation of each PEMWE single-stack for the first 148 h under each power allocation strategy is shown in Fig. 14. In the figure, the curves for each single-stack at the same operating power are overlapping, which should be noted in the analysis. It can be seen that the operation of each single-stack under the average allocation strategy is identical and the power volatility is the same as the wind power. There is a significant difference in the operation of each single-stack in the daisy chain allocation strategy. For example, PEMWE 1 operates first and for the longest time, operating under harsher conditions, while PEMWE 4 is idle for a long time. The power allocation strategy considers optimal efficiency to maintain the efficiency optimum all the time, when the wind power fluctuates in the low power range (e.g., 0–40 h and 80–120 h) the start-stop switching of each single-stack is too frequent. Under the power allocation strategy considering PEMWE degradation designed in this work, the working time and condition of each single-stack are basically the same, and the first working electrolyzer will be ordered backward according to the voltage degradation, taking turns to bear the wind power volatility.

The operating time of each PEMWE single-stack under five operating conditions with different power allocation strategies is shown in Fig. 15. With the average allocation strategy, the operation time for different operating conditions of each single-stack is exactly the same, and operates at low power fluctuations most of the time. The differences in the operation of each single-stack under the optimal efficiency allocation are smaller than under the daisy chain allocation, and the operating time of each single-stack at high power fluctuation is the same because all single-stacks have started up. The operation of each single-stack under the allocation strategy in this work is basically the same, which is consistent with the previous analysis.

The voltage degradation of each PEMWE single-stack under different power allocation strategies is shown in Fig. 16. The voltage degradation of each single-stack under different strategies is obviously different, the cumulative voltage

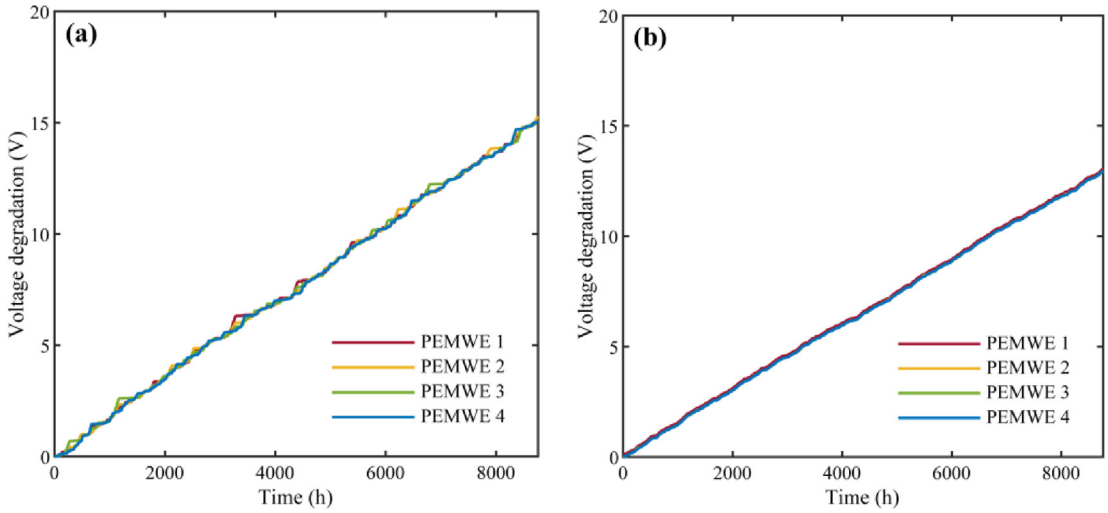

Fig. 17 – Voltage degradation of each PEMWE single-stack under (a) daisy chain allocation and (b) optimal efficiency allocation (after optimization).

degradation of a single-stack in one year is 17.43 V under the average allocation strategy. In the daisy chain allocation strategy, PEMWE 1 has the most serious voltage degradation, which is 34.25 V, and the other single-stacks are reduced in order to startup, which are 15.32 V, 8.55 V, and 2.37 V. The trend of voltage degradation for each single-stack under the optimal efficiency allocation is similar to the daisy chain allocation, but the magnitude is smaller, which are 16.52 V, 13.36 V, 11.15 V, and 9.79 V. Under the allocation strategy in this work, the voltage degradation is basically the same for each single-stack, which is about 7.5 V.

In order to solve the problem of inconsistent voltage degradation for each single-stack in the daisy chain allocation and the optimal efficiency allocation, the power allocation order sorting module designed in this work is added for optimization, and the voltage degradation is shown in Fig. 17. After adding the power allocation order sorting module, the multi-stack consistency is basically ensured, but the voltage degradation is still high, which is 15.1 V under the daisy chain allocation, and 12.9 V under the optimal efficiency allocation. In the subsequent analysis, the operating data under both strategies are the data after adding the power allocation order sorting module.

The PEMWE single-stack efficiency curves under the four strategies after 8760 h of operation are shown in Fig. 18. It can be seen that under the power allocation strategy considering PEMWE degradation, the maximum efficiency of the PEMWE single-stack is 65.28%, which is 6.29% lower than that without degradation, and all other power allocation strategies are more than 10% decrease.

The cumulative energy efficiency of the multi-stack PEMWE array under the four power allocation strategies is shown in Fig. 19. The electrolyzer efficiency is lower under the daisy chain allocation strategy, which has been analyzed in Fig. 8. Therefore, the allocation strategy in this work (about 64%) also has lower energy efficiency at the beginning of system operation, which is slightly higher than the daisy chain allocation strategy (about 63%), but lower compared with other allocation strategies (about 67%).

The efficiency data in Figs. 18 and 19 were collated into Fig. 20. The energy efficiency under the optimal efficiency allocation strategy is the highest, with 61.86%, which is predictable because all the single-stacks operate at the optimal efficiency point at all times. In the daisy chain allocation strategy, due to the low-efficiency curve of the system and the rapid degradation of each single-stack, the cumulative energy efficiency is very low. And under the allocation strategy in this work, due to the slow degradation rate of each single-stack, although the initial energy efficiency of the system is not high, the cumulative energy efficiency of the system reaches 61.65%, which is comparable to the efficiency of the optimal allocation strategy.

In addition, to verify the necessity of a 600 W external power supply, it is assumed that the speed of PEMWE start-up (shutdown) can fully follow the fluctuation of wind power, and frequent start-stop switching doesn't affect the aging. Then there will be no need to set the external power supply, the energy efficiency of the multi-stack PEMWE array under the

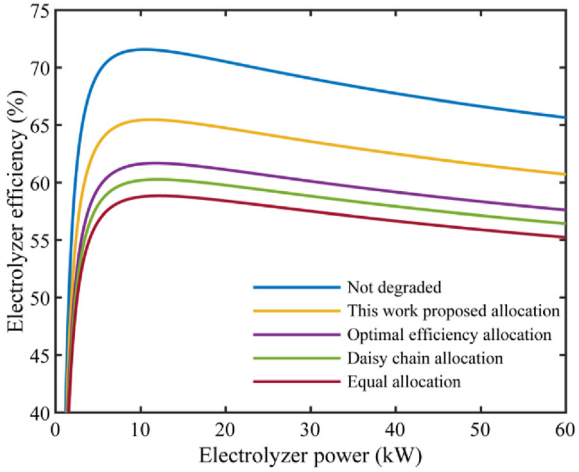

Fig. 18 – PEMWE single-stack efficiency curves under the four strategies after 8760 h of operation.

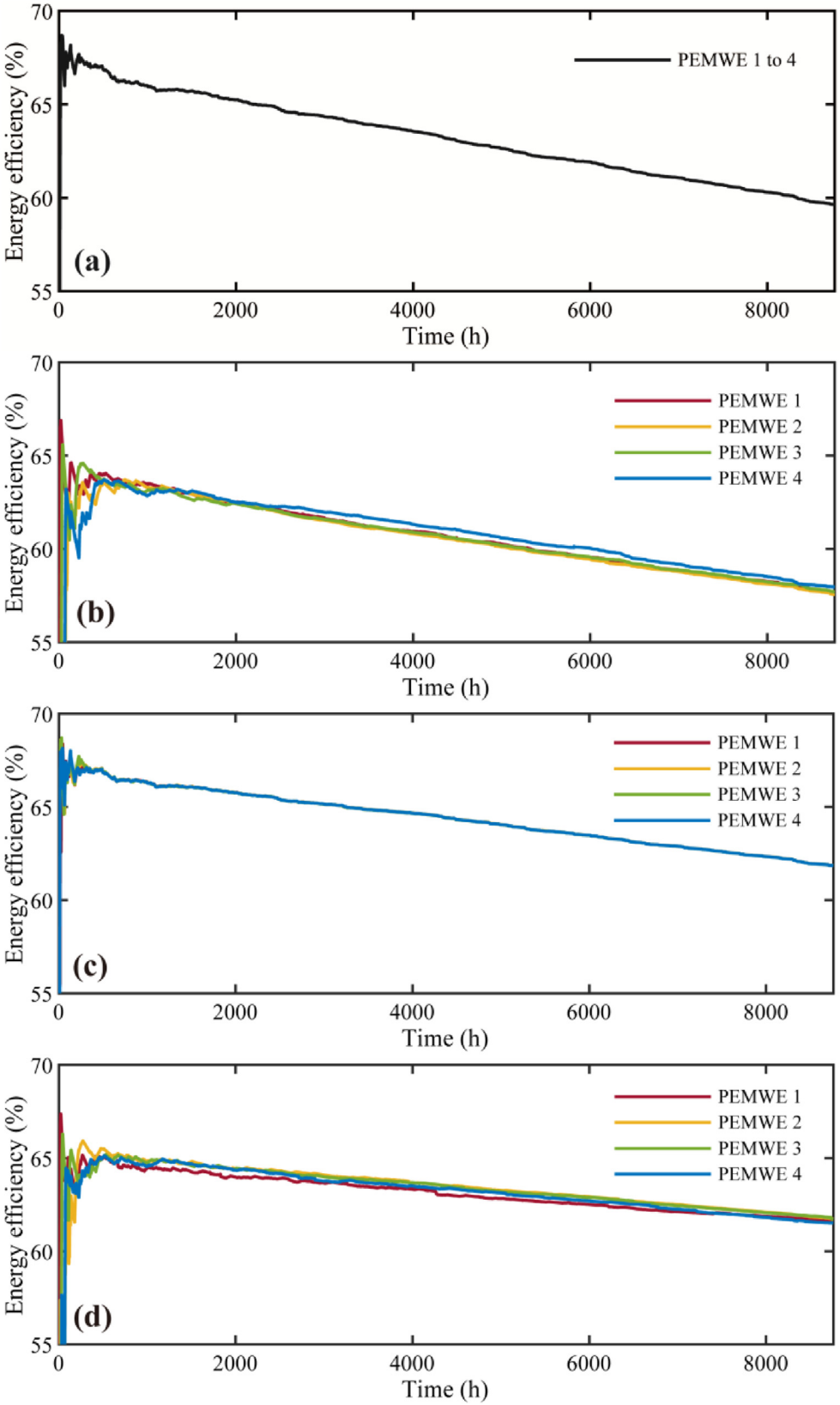

Fig. 19 – The cumulative energy efficiency of the multi-stack PEMWE array under (a) average allocation, (b) daisy chain allocation, (c) optimal efficiency allocation, and (d) proposed allocation strategy.

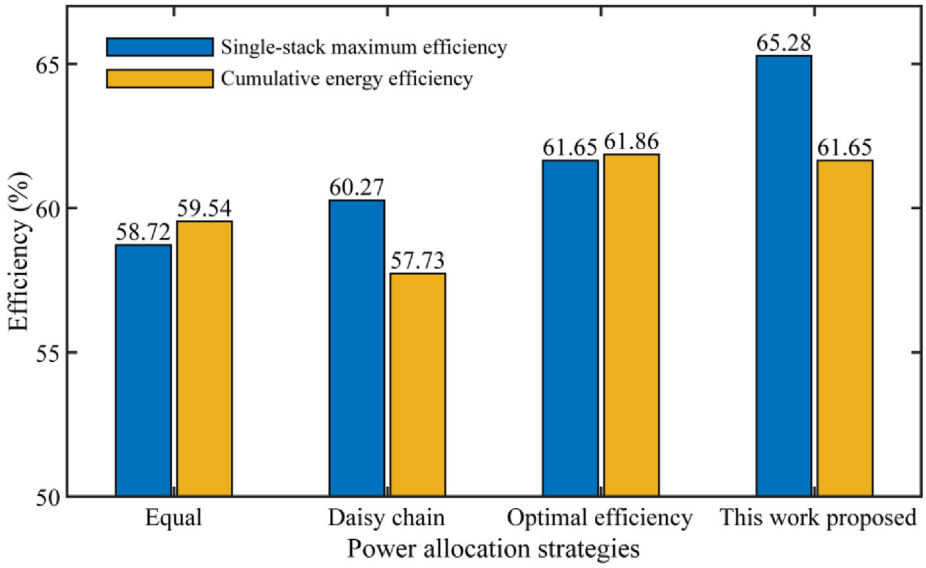

Fig. 20 – Efficiency of PEMWE single-stack and system under the four strategies after 8760 h of operation. Note: Cumulative energy efficiency includes a 600 W external power supply.

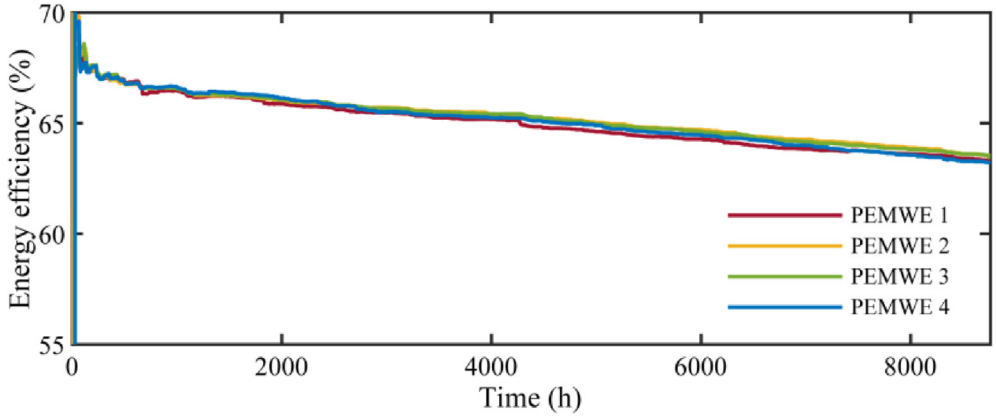

Fig. 21 – Cumulative energy efficiency of the multi-stack PEMWE array without external power supply under the proposed power allocation strategy.

allocation strategy in this work is shown in Fig. 21. Without an external power supply, the cumulative energy efficiency is 63.37%, so the external power supply has less influence on the energy efficiency of the wind-hydrogen system. However, the above assumptions are not valid in actual operation, and the complete start-up (shutdown) of PEMWE requires other auxiliary equipment, which takes a long time. Moreover, as mentioned in Table 3, frequent start-stop switching will accelerate the degradation of the electrolyzer, so setting the external power supply in the wind-hydrogen system is an effective solution for the power following and frequent start-stop switching of PEMWE.

Table 6 – EDCIBC parameters.

Parameters	Value	Unit
f_s	100	kHz
V_{dc}	1	kV
C_1	250	μF
C_2	250	μF
C_3	10	μF
C_4	10	μF
C_o	250	mF
L_1	1	mH
L_2	1	mH

Verification of power allocation execution module

The previous section basically verified the role of the power allocation control module, but the power allocation of the wind-hydrogen system eventually needs to be transformed into a stable hydrogen output, which requires the execution module to fast follow the changes of the power allocation signal and provide high-quality power with low current ripple to each PEMWE, while ensuring the reliability of the converter. This will not be achieved by optimizing the power allocation strategy, and this section will verify the performance of the EDCIBC based on fuzzy PID control as an execution module.

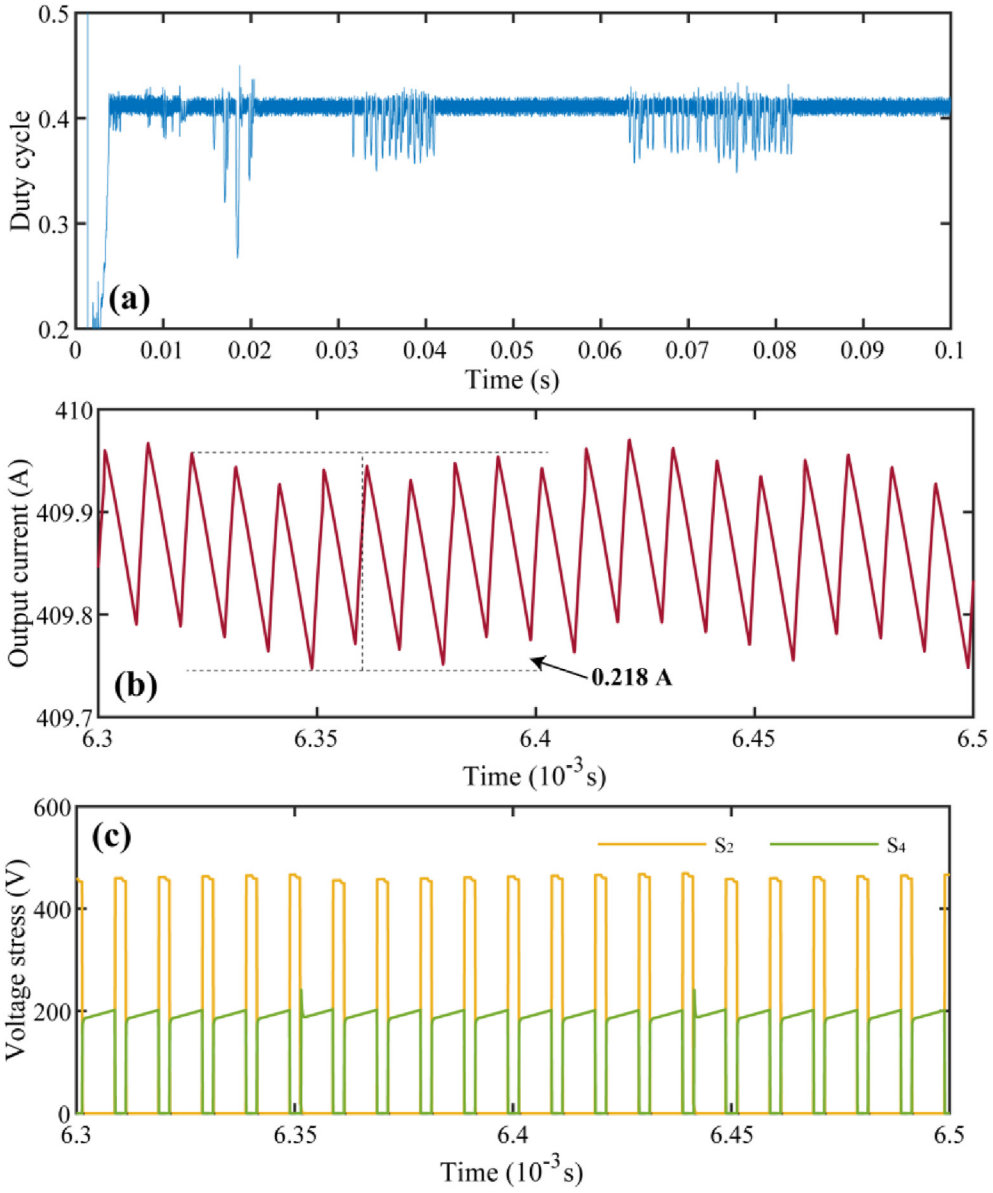

Fig. 22 – Static characteristics of EDCIBC. (a) Duty cycle *D*. (b) Current ripple Δi_o. (c) Switching device voltage stress V_S.

The. EDCIBC parameters are set as shown in Table 6.

When the system allocation power signal $P_{ref} = 40$ kW, the EDCIBC duty cycle *D*, current ripple Δi_o, and switching device voltage stress V_S are shown in Fig. 22.

Comparing the data in the figure with the theoretical data calculated by Eqs. (22)–(24), as shown in Table 7, basically verifies the advantages of the static characteristics of EDCIBC.

Table 7 – Comparison of theoretical and simulated values of EDCIBC static characteristics.

Names	Parameters	Theoretical value	Simulated value
Duty cycle	*D*	0.39	0.41
Current ripple	Δi_o (A)	0.215	0.218
Switching device voltage stress	V_{S2} (V)	500	475.8
	V_{S4} (V)	250	240.9

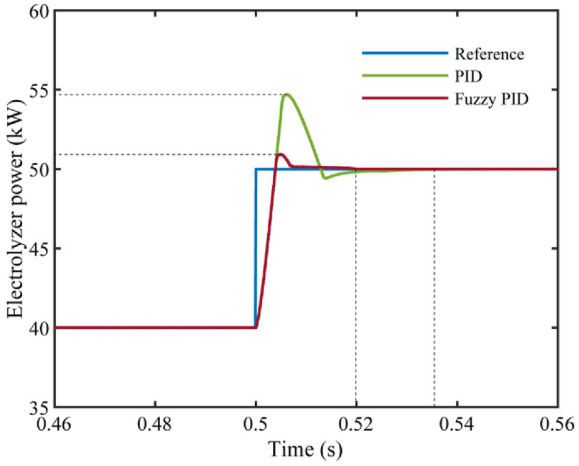

Fig. 23 – EDCIBC output power response curve based on conventional PID control and fuzzy PID control.

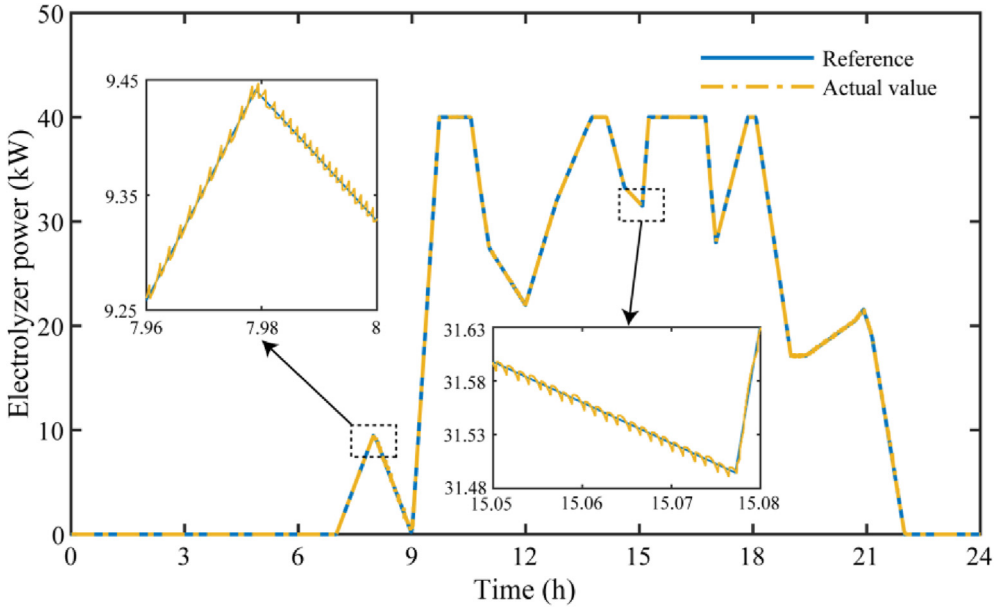

Fig. 24 – The dynamic characteristics of EDCIBC (24 h).

Setting the P_{ref} to step from 40 kW to 50 kW in 0.5 s, the EDCIBC output power response curve based on conventional PID control and fuzzy PID control is shown in Fig. 23. It can be seen that the EDCIBC output power based on fuzzy PID control has obvious advantages, the transient time is about 19 ms, which is only 53% of the conventional PID control, and the overshoot is 9.23%, which is only 20.5% of the conventional PID control, fulfilling the requirement of fast and steadily.

The first 24 h power allocation value (blue line) of PEMWE (1) based on the allocation strategy of this work in Fig. 14(a) is used as P_{ref} input to the execution module, as shown in Fig. 24. The EDCIBC output power value basically overlaps with the power allocation signal, and the current ripple is small, which verifies the feasibility and superiority of the EDCIBC based on fuzzy PID control as the power allocation strategy execution module of the wind-hydrogen system.

Conclusion

In this paper, an optimization of power allocation for wind-hydrogen system multi-stack PEM water electrolyzer (PEMWE) considering degradation conditions is proposed. The main findings are concluded as follows.

1) A multi-physics fields three-dimensional model of the PEMWE single-cell was established. From the model analysis, we know that the PEMWE efficiency has a maximum value. With the increase in operation time, PEMWE will have voltage degradation. The voltage degradation rate is different under different operating conditions, and the voltage degradation becomes more serious, and the hydrogen production efficiency becomes lower.
2) Power allocation control module. In 8760 h of operation, the cumulative energy efficiency of the wind-hydrogen system reached 61.65%, which is comparable to the power allocation strategy considering optimal efficiency. Meanwhile, the PEMWE single-stack voltage degradation is 7.5 V, and the maximum efficiency is 6.29% lower than that without degradation, both of which are better than other power allocation strategies.
3) Power allocation execution module. The EDCIBC based on fuzzy PID control has great bucking capability and output power quality. The current ripple amplitude is only 0.053% of the output current, and the switching device voltage stress is up to 50% of the input voltage. Compared with conventional PID control, the transient time is shortened by 53%, the overshoot is shortened by 79.5%, and the power allocation signal can be followed fast and steadily.

The optimization method proposed in this work effectively slows down the degradation of the multi-stack PEMWE array and improves the system energy efficiency, which has practical significance for the large-scale application of wind-hydrogen systems. However, it should be noted that the size of the external power supply power and the turning power point P_t of the system need to be determined based on the performance and operating conditions of the PEMWE in the actual application. In addition, the method is also applicable to AE, AEMWE and SOE, and its general applicability will be verified in future work.

Declaration of competing interest

The authors declare that they have no known competing financial interests or personal relationships that could have appeared to influence the work reported in this paper.

Acknowledgment

This paper is supported by the National Key Research and Development Program of China (No. 2020YFB1506802) and the Fundamental Research Funds for the Central Universities (WUT:2021IVA120).

REFERENCES

[1] Gao C, Sun M, Geng Y, Wu R, Chen W. A bibliometric analysis based review on wind power price. Appl Energy 2016;182:602–12. https://doi.org/10.1016/j.apenergy.2016.08.144.
[2] Global Wind Energy Council. Global offshore wind power report 2022. 2022. https://gwec.net/gwecs-global-offshore-wind-report/. [Accessed 24 August 2022].
[3] Ren G, Liu J, Wan J, Guo Y, Yu D. Overview of wind power intermittency: impacts, measurements, and mitigation solutions. Appl Energy 2017;204:47–65. https://doi.org/10.1016/j.apenergy.2017.06.098.
[4] Glenk G, Reichelstein S. Economics of converting renewable power to hydrogen. Nat Energy 2019;4. https://doi.org/10.1038/s41560-019-0367-5. 347-347.
[5] Nagasawa K, Davidson FT, Lloyd AC, Webber ME. Impacts of renewable hydrogen production from wind energy in electricity markets on potential hydrogen demand for light-duty vehicles. Appl Energy 2019;235:1001–16. https://doi.org/10.1016/j.apenergy.2018.10.067.
[6] He W, Abbas Q, Alharthi M, Mohsin M, Hanif I, Xuan Vinh V, et al. Integration of renewable hydrogen in light-duty vehicle: nexus between energy security and low carbon emission resources. Int J Hydrogen Energy 2020;45:27958–68. https://doi.org/10.1016/j.ijhydene.2020.06.177.
[7] Olateju B, Kumar A, Secanell M. A techno-economic assessment of large scale wind-hydrogen production with energy storage in Western Canada. Int J Hydrogen Energy 2016;41:8755–76. https://doi.org/10.1016/j.ijhydene.2016.03.177.
[8] Xiao P, Hu W, Xu X, Liu W, Huang Q, Chen Z. Optimal operation of a wind-electrolytic hydrogen storage system in the electricity/hydrogen markets. Int J Hydrogen Energy 2020;45:24412–23. https://doi.org/10.1016/j.ijhydene.2020.06.302.
[9] Kudria S, Ivanchenko I, Tuchynskyi B, Petrenko K, Karmazin O, Riepkin O. Resource potential for wind-hydrogen power in Ukraine. Int J Hydrogen Energy 2021;46:157–68. https://doi.org/10.1016/j.ijhydene.2020.09.211.
[10] Wang X, Li B, Wang Y, Lu H, Zhao H, Xue W. A bargaining game-based profit allocation method for the wind-hydrogen-storage combined system. Appl Energy 2022;310. https://doi.org/10.1016/j.apenergy.2021.118472.
[11] Pein M, Neumann NC, Venstrom LJ, Vieten J, Roeb M, Sattler C. Two-step thermochemical electrolysis: an approach for green hydrogen production. Int J Hydrogen Energy 2021;46:24909–18. https://doi.org/10.1016/j.ijhydene.2021.05.036.
[12] Buttler A, Spliethoff H. Current status of water electrolysis for energy storage, grid balancing and sector coupling via power-to-gas and power-to-liquids: a review. Renew Sustain Energy Rev 2018;82:2440–54. https://doi.org/10.1016/j.rser.2017.09.003.
[13] Hernandez-Gomez A, Ramirez V, Guilbert D. Investigation of PEM electrolyzer modeling: electrical domain, efficiency, and specific energy consumption. Int J Hydrogen Energy 2020;45:14625–39. https://doi.org/10.1016/j.ijhydene.2020.03.195.
[14] Falcao DS, Pinto AMFR. A review on PEM electrolyzer modelling: guidelines for beginners. J Clean Prod 2020;261. https://doi.org/10.1016/j.jclepro.2020.121184.
[15] Caparros Mancera JJ, Segura Manzano F, Manuel Andujar J, Jose Vivas F, Jose Calderon A. An optimized balance of plant for a medium-size PEM electrolyzer: design, control and physical implementation. Electron 2020;9. https://doi.org/10.3390/electronics9050871.
[16] Park JE, Kang SY, Oh SH, Kim JK, Lim MS, Ahn CY, et al. High-performance anion-exchange membrane water electrolysis. Electrochim Acta 2019;295:99–106. https://doi.org/10.1016/j.electacta.2018.10.143.
[17] Kang SY, Park JE, Jang GY, Kim OH, Kwon OJ, Cho YH, et al. High-performance and durable water electrolysis using a highly conductive and stable anion-exchange membrane. Int J Hydrogen Energy 2022;47:9115–26. https://doi.org/10.1016/j.ijhydene.2022.01.002.
[18] Motealleh B, Liu ZC, Masel RI, Sculley JP, Ni ZR, Meroueh L. Next-generation anion exchange membrane water electrolyzers operating for commercially relevant lifetimes. Int J Hydrogen Energy 2021;46:3379–86. https://doi.org/10.1016/j.ijhydene.2020.10.244.
[19] Panah PG, Cui XT, Bornapour M, Hooshmand RA, Guerrero JM. Marketability analysis of green hydrogen production in Denmark: scale-up effects on grid- connected electrolysis. Int J Hydrogen Energy 2022;47:12443–55. https://doi.org/10.1016/j.ijhydene.2022.01.254.
[20] AlZahrani AA, Dincer I. Thermodynamic and electrochemical analyses of a solid oxide electrolyzer for hydrogen production. Int J Hydrogen Energy 2017;42:21404–13. https://doi.org/10.1016/j.ijhydene.2017.03.186.
[21] Cao F, Guo T, Chen K, Jin X, Zhang L, Yang J, et al. Progress and development prospect of coupled wind and hydrogen systems. Proc Chin Soc Electr Eng 2021;41:2187–200. https://doi.org/10.13334/j.0258-8013.pcsee.200452.
[22] Feng Q, Yuan X-Z, Liu G, Wei B, Zhang Z, Li H, et al. A review of proton exchange membrane water electrolysis on degradation mechanisms and mitigation strategies. J Power Sources 2017;366:33–55. https://doi.org/10.1016/j.jpowsour.2017.09.006.
[23] Khatib FN, Wilberforce T, Ijaodola O, Ogungbemi E, El-Hassan Z, Durrant A, et al. Material degradation of components in polymer electrolyte membrane (PEM) electrolytic cell and mitigation mechanisms: a review. Renew Sustain Energy Rev 2019;111:1–14. https://doi.org/10.1016/j.rser.2019.05.007.
[24] Chandesris M, Medeau V, Guillet N, Chelghoum S, Thoby D, Fouda-Onana F. Membrane degradation in PEM water electrolyzer: numerical modeling and experimental evidence of the influence of temperature and current density. Int J Hydrogen Energy 2015;40:1353–66. https://doi.org/10.1016/j.ijhydene.2014.11.111.
[25] Frensch SH, Fouda-Onana F, Serre G, Thoby D, Araya SS, Kaer SK. Influence of the operation mode on PEM water electrolysis degradation. Int J Hydrogen Energy 2019;44:29889–98. https://doi.org/10.1016/j.ijhydene.2019.09.169.
[26] Weiss A, Siebel A, Bernt M, Shen TH, Tileli V, Gasteiger HA. Impact of intermittent operation on lifetime and performance of a PEM water electrolyzer. J Electrochem Soc 2019;166:F487–97. https://doi.org/10.1149/2.0421908jes.

[27] Hartig-Weiss A, Bernt M, Siebel A, Gasteiger HA. A platinum micro-reference electrode for impedance measurements in a PEM water electrolysis cell. J Electrochem Soc 2021;168. https://doi.org/10.1149/1945-7111/ac3717.
[28] Rakousky C, Reimer U, Wippermann K, Kuhri S, Carmo M, Lueke W, et al. Polymer electrolyte membrane water electrolysis: restraining degradation in the presence of fluctuating power. J Power Sources 2017;342:38–47. https://doi.org/10.1016/j.jpowsour.2016.11.118.
[29] Guo X, Wei Y, Wan Y, Zhou Y, Kong L, Zhang Z, et al. Review on power electronic converters for producing hydrogen from renewable energy sources. Autom Electr Power Syst 2021;45:185–99. https://doi.org/10.7500/AEPS20201101004.
[30] Marx N, Boulon L, Gustin F, Hissel D, Agbossou K. A review of multi-stack and modular fuel cell systems: interests, application areas and on-going research activities. Int J Hydrogen Energy 2014;39:12101–11. https://doi.org/10.1016/j.ijhydene.2014.05.187.
[31] Muyeen SM, Takahashi R, Tamura J. Electrolyzer switching strategy for hydrogen generation from variable speed wind generator. Elec Power Syst Res 2011;81:1171–9. https://doi.org/10.1016/j.epsr.2011.01.005.
[32] Fang R, Liang Y. Control strategy of electrolyzer in a wind-hydrogen system considering the constraints of switching times. Int J Hydrogen Energy 2019;44:25104–11. https://doi.org/10.1016/j.ijhydene.2019.03.033.
[33] Hong Z, Wei Z, Han X. Optimization scheduling control strategy of wind-hydrogen system considering hydrogen production efficiency. J Energy Storage 2022;47. https://doi.org/10.1016/j.est.2021.103609.
[34] Luxa A, Jores N, Yanez CC, Souza MN, Pangalos G, Schnelle L, et al. Multilinear modeling and simulation of a multi-stack PEM electrolyzer with degradation for control concept comparison. In: Proceedings of the 12th international conference on simulation and modeling methodologies, technologies and applications (simultech) 2022; 2022. p. 52–62. https://doi.org/10.5220/0011263300003274.
[35] Guo X, Zhang S, Liu Z, Sun L, Lu Z, Hua C, et al. A new multi-mode fault-tolerant operation control strategy of multiphase stacked interleaved Buck converter for green hydrogen production. Int J Hydrogen Energy 2022;47:30359–70. https://doi.org/10.1016/j.ijhydene.2022.06.249.
[36] Guilbert D, Collura SM, Scipioni A. DC/DC converter topologies for electrolyzers: state-of-the-art and remaining key issues. Int J Hydrogen Energy 2017;42:23966–85. https://doi.org/10.1016/j.ijhydene.2017.07.174.
[37] Pan C-T, Chuang C-F, Chu C-C. A novel transformerless interleaved high step-down conversion ratio DC-DC converter with low switch voltage stress. IEEE Trans Ind Electron 2014;61:5290–9. https://doi.org/10.1109/TIE.2014.2301774.
[38] Deng Z, Jiang Y. Optimal sizing of wind-hydrogen system considering hydrogen demand and trading modes. Int J Hydrogen Energy 2020;45:11527–37. https://doi.org/10.1016/j.ijhydene.2020.02.089.
[39] Jiang Y, Deng Z, You S. Size optimization and economic analysis of a coupled wind-hydrogen system with curtailment decisions. Int J Hydrogen Energy 2019;44:19658–66. https://doi.org/10.1016/j.ijhydene.2019.06.035.
[40] Rahim AHA, Tijani AS, Kamarudin SK, Hanapi S. An overview of polymer electrolyte membrane electrolyzer for hydrogen production: modeling and mass transport. J Power Sources 2016;309:56–65. https://doi.org/10.1016/j.jpowsour.2016.01.012.
[41] Han B, Steen III M, Mo J, Zhang F-Y. Electrochemical performance modeling of a proton exchange membrane electrolyzer cell for hydrogen energy. Int J Hydrogen Energy 2015;40:7006–16. https://doi.org/10.1016/j.ijhydene.2015.03.164.
[42] Abdin Z, Webb CJ, Gray EM. Modelling and simulation of a proton exchange membrane (PEM) electrolyser cell. Int J Hydrogen Energy 2015;40:13243–57. https://doi.org/10.1016/j.ijhydene.2015.07.129.
[43] Aubras F, Deseure J, Kadjo JJA, Dedigama I, Majasan J, Grondin-Perez B, et al. Two-dimensional model of low-pressure PEM electrolyser: two-phase flow regime, electrochemical modelling and experimental validation. Int J Hydrogen Energy 2017;42:26203–16. https://doi.org/10.1016/j.ijhydene.2017.08.211.
[44] Toghyani S, Afshari E, Baniasadi E. Metal foams as flow distributors in comparison with serpentine and parallel flow fields in proton exchange membrane electrolyzer cells. Electrochim Acta 2018;290:506–19. https://doi.org/10.1016/j.electacta.2018.09.106.
[45] Chen Y, Mojica F, Li G, Chuang P-YA. Experimental study and analytical modeling of an alkaline water electrolysis cell. Int J Energy Res 2017;41:2365–73. https://doi.org/10.1002/er.3806.
[46] Toghyani S, Afshari E, Baniasadi E, Atyabi SA. Thermal and electrochemical analysis of different flow field patterns in a PEM electrolyzer. Electrochim Acta 2018;267:234–45. https://doi.org/10.1016/j.electacta.2018.02.078.
[47] Ojong ET, Kwan JTH, Nouri-Khorasani A, Bonakdarpour A, Wilkinson DP, Smolinka T. Development of an experimentally validated semi-empirical fully-coupled performance model of a PEM electrolysis cell with a 3-D structured porous transport layer. Int J Hydrogen Energy 2017;42:25831–47. https://doi.org/10.1016/j.ijhydene.2017.08.183.
[48] Kaya MF, Demir N. Numerical investigation of PEM water electrolysis performance for different oxygen evolution electrocatalysts. Fuel Cell 2017;17:37–47. https://doi.org/10.1002/fuce.201600216.
[49] Tugirumubano A, Shin H-J, Go S-H, Lee M-S, Kwac LK, Kim H-G. Electrochemical performance analysis of a PEM water electrolysis with cathode feed mode based on flow passage shape of titanium plates. Int J Precis Eng Manuf 2016;17:1073–8. https://doi.org/10.1007/s12541-016-0130-9.
[50] Schalenbach M, Carmo M, Fritz DL, Mergel J, Stolten D. Pressurized PEM water electrolysis: efficiency and gas crossover. Int J Hydrogen Energy 2013;38:14921–33. https://doi.org/10.1016/j.ijhydene.2013.09.013.
[51] Grigoriev SA, Porembskiy VI, Korobtsev SV, Fateev VN, Aupretre F, Millet P. High-pressure PEM water electrolysis and corresponding safety issues. Int J Hydrogen Energy 2011;36:2721–8. https://doi.org/10.1016/j.ijhydene.2010.03.058.
[52] Yodwong B, Guilbert D, Phattanasak M, Kaewmanee W, Hinaje M, Vitale G. Faraday's efficiency modeling of a proton exchange membrane electrolyzer based on experimental data. Energies 2020;13. https://doi.org/10.3390/en13184792.
[53] Babic U, Suermann M, Buechi FN, Gubler L, Schmidt TJ. Review-identifying critical gaps for polymer electrolyte water electrolysis development. J Electrochem Soc 2017;164:F387–99. https://doi.org/10.1149/2.1441704jes.
[54] Mohammadi A, Mehrpooya M. A comprehensive review on coupling different types of electrolyzer to renewable energy sources. Energy 2018;158:632–55. https://doi.org/10.1016/j.energy.2018.06.073.
[55] Rakousky C, Reimer U, Wippermann K, Carmo M, Lueke W, Stolten D. An analysis of degradation phenomena in polymer electrolyte membrane water electrolysis. J Power Sources 2016;326:120–8. https://doi.org/10.1016/j.jpowsour.2016.06.082.
[56] Guilbert D, N'Diaye A, Luberda P, Djerdir A. Fuel cell lifespan optimization by developing a power switch fault-tolerant

control in a floating interleaved boost converter. Fuel Cell 2017;17:196–209. https://doi.org/10.1002/fuce.201600058.

[57] Daud WRW, Rosli RE, Majlan EH, Hamid SAA, Mohamed R, Husaini T. PEM fuel cell system control: a review. Renew Energy 2017;113:620–38. https://doi.org/10.1016/j.renene.2017.06.027.

[58] Yang B, Li JL, Li YL, Guo ZX, Zeng KD, Shu HC, et al. A critical survey of proton exchange membrane fuel cell system control: summaries, advances, and perspectives. Int J Hydrogen Energy 2022;47:9986–10020. https://doi.org/10.1016/j.ijhydene.2022.01.065.